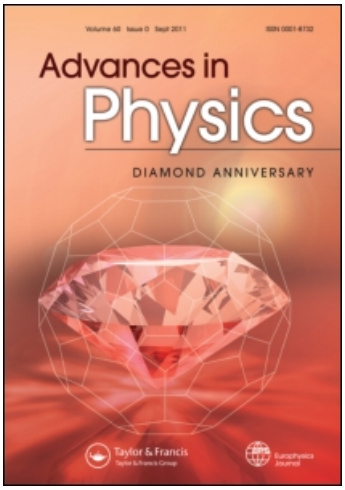

Advances in Physics
Publication details, including instructions for authors and subscription information:
http://www.informaworld.com/smpp/title~content=t713736250

Scale invariance in plastic flow of crystalline solids

Michael Zaiser[a]
[a] The University of Edinburgh, Institute for Materials and Processes, Edinburgh EH9 3JL, UK

To cite this Article Zaiser, Michael(2006) 'Scale invariance in plastic flow of crystalline solids', Advances in Physics, 55: 1, 185 — 245
To link to this Article: DOI: 10.1080/00018730600583514
URL: http://dx.doi.org/10.1080/00018730600583514

Advances in Physics,
Vol. 55, Nos. 1–2, January–April 2006, 185–245

Taylor & Francis
Taylor & Francis Group

Scale invariance in plastic flow of crystalline solids

MICHAEL ZAISER*

The University of Edinburgh, Institute for Materials and Processes,
The King's Buildings, Sanderson Building, Edinburgh EH9 3JL, UK

(*Received 31 October 2005; in final form 17 January 2006*)

From the traditional viewpoint of continuum plasticity, plastic deformation of crystalline solids is, at least in the absence of so-called plastic instabilities, envisaged as a smooth and quasi-laminar flow process. Recent theoretical and experimental investigations, however, demonstrate that crystal plasticity is characterized by large intrinsic spatio-temporal fluctuations with scale-invariant characteristics: In time, deformation proceeds through intermittent bursts with power-law size distributions; in space, deformation patterns and deformation-induced surface morphology are characterized by long-range correlations, self-similarity and/or self-affine roughness. We discuss this scale-invariant behaviour in terms of robust scaling associated with a non-equilibrium critical point ('yielding transition').

Contents

*Email: m.zaiser@ed.ac.uk

Advances in Physics
ISSN 0001–8732 print/ISSN 1460–6976 online
http://www.tandf.co.uk/journals
DOI: 10.1080/00018730600583514

1. Introduction

According to the traditional paradigm implicit in continuum models of plasticity, crystalline solids are considered as homogeneous continua which, in the absence of so-called plastic instabilities, deform under homogeneous loads in a smooth and spatially homogeneous manner. Fluctuations are supposed to average out above the scale of a 'representative volume element' which is assumed to be small in comparison with the dimensions of the deforming body. Spatio-temporal deformation patterning may, according to this viewpoint, occur only if the deformation process is macroscopically unstable due to some mechanism which produces strain or strain rate softening. Macroscopic plastic instabilities of this type give rise to spatio-temporal patterns in the form of stationary or travelling solitary waves (see, e.g. the *Scripta Materialia* Viewpoint set edited by Kubin, Estrin and Aifantis [1]) and to oscillatory and/or chaotic deformation modes (see the reviews by Zaiser and Hähner [2] and by Kubin, Fressengeas and Ananthakrishna [3]). These phenomena have been studied in some detail in conjunction with the general enthusiasm for nonlinear phenomena in the 1980s and early 1990s, but were generally looked upon as representing some kind of scientifically interesting, but non-generic behaviour, out of the ordinary and of limited practical importance.

The paradigm of plastic flow as a smooth process has a counterpart in the work of materials scientists investigating the micromechanisms of crystal plasticity, *viz*., the motion of the line defects (dislocations) which in a crystal lattice carry discrete 'quanta' of slip. Due to the discreteness of dislocations, plastic flow on the 'microscopic' scale of individual dislocations is necessarily inhomogeneous in space and often, due to the presence of localized obstacles, intermittent in time. However, in line with the continuum paradigm, the prevailing viewpoint was that microscopic deformation localization and intermittency are irrelevant as soon as multiple defects are involved, since the incoherent superposition of individual defect motions would result in a smooth and approximately homogeneous flow. It is an assumption implicit in much of the materials science work on plasticity that lack of coherency in the individual defect processes leads to deformation behaviour that is statistically homogenous on the mesoscopic scale of multiple defects. This assumption is also convenient from a modelling viewpoint, since it allows us to draw direct conclusions from the properties of individual defects, or from their pair interactions, on the macroscopic material behaviour.

Recently, however, the traditional paradigm of 'stable' plastic deformation as a smooth and steady flow process has been challenged both from an experimental and from a theoretical point of view (see, e.g. [4–8]). From these works, a quite different picture of plastic flow emerges: Instead of the incoherent motion of individual

defects, one finds coherent bursts of activity with long-range correlations both in space and in time. Such correlated bursts are detected in situations where the traditional paradigm leads one to expect to find a smooth and homogeneous flow. The properties of these bursts also differ from those commonly associated with plastic instabilities: Instead of coherent spatio-temporal oscillations one finds random bursts with scale-free size distributions, instead of plastic wave propagation one sees long-range correlated deformation patterns with self-similar or self-affine characteristics, and instead of the emergence of characteristic internal length and time scales one observes scale-free behaviour in space and in time. In short, the picture is that of critical phenomena commonly associated with phase transitions, rather than that of coherent nonlinear behaviour.

In the present review we summarize experimental and theoretical work on the (almost) scale-free fluctuation phenomena that can be observed in deforming crystals. In the rest of the introduction, we give a brief summary of continuum mechanics approaches towards crystal plasticity, which mainly serves to introduce relevant terminology used by the continuum mechanics community. We also discuss the yielding of a crystal on the dislocation level (dislocation depinning); in this context we present the reader with a set of phenomena that have been studied by statistical physicists in the general context of the dynamics of elastic manifolds in random media, and which will recur in one form or another throughout the subsequent chapters. In our section on experimental observations, we discuss in some detail acoustic emission (AE) measurements which are possibly the most useful available tool for monitoring the temporal dynamics of plastic flow *in situ*. We also discuss the surface-based *in situ* and post mortem investigation of deformation patterns based on the study of traces of dislocation motion (slip lines), and the analysis of deformation-induced changes in the overall surface morphology (surface roughening). We then discuss the theoretical modelling of flow phenomena in terms of the dynamics of interacting dislocations, in terms of phenomenological continuum models describing the evolution of plastic strain above the dislocation scale, and in terms of phase-field models which in a sense are in between the former two approaches. We demonstrate that these approaches result in a consistent picture of the main characteristics of the 'yielding transition' which can qualitatively or semi-quantitatively account for many of the pertinent experimental observations, though several open questions remain. It is important to note that the present review does not account for all types of scale-free behaviour in plastically deforming crystals: We exclude the entire realm of plastic instabilities, in particular the scale-free statistics of load drops associated with the so-called PLC effect [3]. We also exclude from our discussion the scale-free defect microstructures which emerge during deformation of crystals in certain high-symmetry orientations [9, 10] but are absent under other deformation conditions and may, hence, represent a non-generic feature.

1.1. *Continuum mechanics of crystal plasticity*

We first discuss the conventional continuum mechanics approach towards crystal plasticity. Besides illustrating the pertinent concepts and mindset, this serves to

introduce a set of notations that will structure our discussion throughout the present review.

Plasticity, reversible and irreversible deformation Plastic deformation can be loosely defined as any deformation of a solid body that persists after the driving force applied to the deforming body is removed. Of necessity this implies changes in neighbourhood relations between atoms. In general, plasticity is isochoric, i.e. the volume of the deforming body is not changed. Plastic deformation is always an irreversible process in the thermodynamic sense, but conversely not every thermodynamically irreversible deformation process is plastic: viscoelastic behaviour dissipates energy, even though the initial shape of the body is restored once the forces are removed (no plasticity), viscous flow of a liquid entails both dissipation and an irreversible change in shape, but the deforming body is not solid (i.e. it does not possess a finite yield stress, cf. below). In a plastically deforming solid, we may split the total strain tensor $\boldsymbol{\epsilon}$ into an elastic and a plastic part. Throughout this paper we adopt a small-strain formulation, such that an additive decomposition is feasible:

$$\boldsymbol{\epsilon} = \boldsymbol{\epsilon}^{\mathrm{el}} + \boldsymbol{\epsilon}^{\mathrm{pl}}. \tag{1}$$

In a linearly elastic material the elastic strain is related to the stress $\boldsymbol{\Sigma}$ via $\boldsymbol{\epsilon}^{\mathrm{el}} = \mathbf{C}^{-1}\boldsymbol{\Sigma}$ where $\mathbf{C}$ is Hooke's tensor of elastic moduli. If the stress is removed, the plastic strain $\boldsymbol{\epsilon}^{\mathrm{pl}}$ remains.

Crystal plasticity, crystallographic slip Plasticity of crystalline solids is constrained by the fact that any occurring atomic rearrangements must preserve the crystal lattice structure. (We exclude from our discussion transformation-induced plasticity, where deformation is due to a stress-driven transition between crystalline phases with *different* lattice structures.) This implies that deformation must occur by shear of adjacent lattice planes such that the displacement of one plane against the other is by a lattice vector contained in the plane. A set of crystallographic planes characterized by their common unit normal vector $\mathbf{n}$, and a corresponding lattice vector $\mathbf{b}$ (also called the *Burgers vector*), constitute a *slip system*. In most crystals, deformation is observed on a small number of slip systems only, often corresponding to the most densely packed planes and lattice directions (e.g. deformation of face-centred cubic crystals occurs usually on slip systems of the type {111}[110]).

The plastic strain tensor $\boldsymbol{\epsilon}^{\mathrm{pl}}$ can be built out of the shear strains on the different slip systems:

$$\boldsymbol{\epsilon}^{\mathrm{pl}} = \sum_i \gamma^{(i)}\mathbf{M}^{(i)}, \quad \mathbf{M}^{(i)} = \frac{1}{2b}\left[\mathbf{b}^{(i)} \otimes \mathbf{n}^{(i)} + \mathbf{n}^{(i)} \otimes \mathbf{b}^{(i)}\right]. \tag{2}$$

Here the index i distinguishes the different slip systems, $\gamma^{(i)}$ are the respective scalar shear strains, and b is the modulus of the Burgers vector (for simplicity assumed the same for all slip systems). The projection tensors $\mathbf{M}^{(i)}$ are symmetrized tensor products of unit vectors in the respective slip plane normal and slip directions.

The driving force for slip on a given slip system is the respective *resolved shear stress* $\tau^{(i)}$, which is the inner product of the stress tensor $\boldsymbol{\Sigma}$ and the projection tensor $\mathbf{M}^{(i)}$:

$$\tau^{(i)} = \mathbf{M}^{(i)} \circ \boldsymbol{\Sigma}. \tag{3}$$

To specify the elastic–plastic material behaviour, one has to provide *constitutive relations* which relate the stress to the plastic strain and possibly to the strain rate and other variables. In crystal plasticity, these are relations between scalar variables (shear strains, resolved shear stresses). To avoid cumbersome notation, in the following we adopt a strictly scalar formulation by focusing on shear deformation on a single slip system. Accordingly, we drop the superscript (i).

Constitutive relations The simplest elastic–plastic models continue the elastic stress–strain relation into a relationship between the stress and the strain in the plastic regime. The basic type of such *rate-independent* constitutive models is commonly called *ideal plasticity* (figure 1, left). In this case, the plastic strain in a material element remains zero unless the stress reaches a critical value τ_y (yield stress) and then increases indefinitely. This corresponds to the assumption of a material that cannot support any shear stresses above the yield stress: at yield the solid effectively turns into an ideal fluid; upon unloading it immediately re-assumes the properties of a linear elastic solid, while the permanent shear deformation remains (dashed line in figure 1, left).

A generalization of this type of constitutive behaviour is to assume that, in the plastic regime, the stress required to deform a material is an increasing function of strain (*strain hardening*). In the stress–strain graph the onset of plasticity in this case corresponds to a change in slope (figure 1, right). The slope of the stress–strain graph $\tau(\gamma)$ in the plastic regime is called the *strain hardening coefficient* θ or, in continuum mechanics language, the tangent modulus. Again, it is important to keep in mind that the elastic and plastic regimes not only differ in the slope of the stress–strain graph, but that the physical processes are fundamentally different (reversible vs. irreversible deformation), as becomes again evident upon unloading (dashed line in figure 1, right).

A different class of models considers plasticity as a time-dependent flow process. *Linear viscoplasticity* assumes that the shear strain rate $\dot{\gamma}$ is zero up to a critical stress (again the yield stress) and then increases linearly with stress (figure 2):

$$\dot{\gamma} = \frac{1}{\mu} \begin{cases} (|\tau| - \tau_y)\,\mathrm{sign}(\tau), & |\tau| > \tau_y, \\ 0 & \text{else.} \end{cases} \tag{4}$$

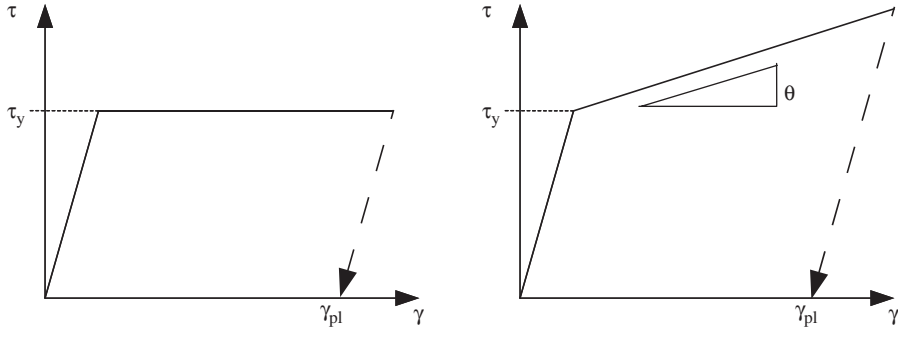

Figure 1. Different types of rate-independent plasticity; left: 'ideally plastic' behaviour; right: plasticity with strain hardening.

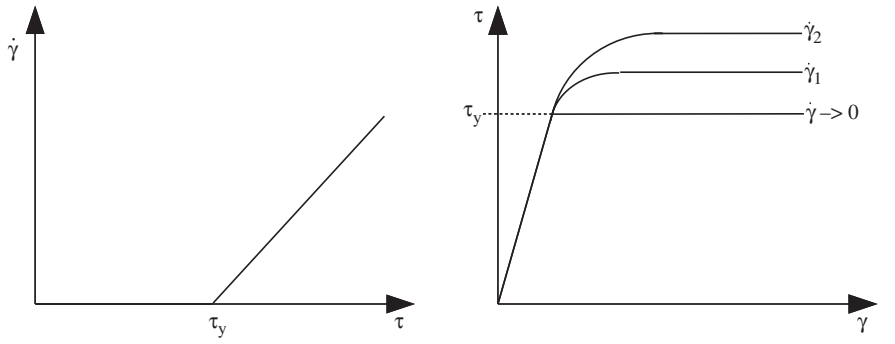

Figure 2. Linear viscoplasticity; left: strain rate vs. stress; right: stress–strain curves for driving at different rates $\dot\gamma_1 > \dot\gamma_2$.

In this equation, the sign function indicates that the direction of shearing is dictated by the sign of the driving stress, whereas the velocity depends on the excess of the driving over the yield stress. μ is a viscoplastic rate coefficient. A viscoelastic solid behaves like a solid for stresses below and like a Newtonian liquid for stresses above the yield stress ('yield-stress liquid').

In a viscoplastic solid, the stress required for deformation is a function of the deformation rate ('flow stress'). In particular, if we impose a constant deformation rate $\dot\gamma_0$, from equation (4) the stress for steady-state deformation becomes

$$\tau_f(\dot\gamma) = \tau_y + \mu\dot\gamma_0, \tag{5}$$

i.e. the flow stress increases with increasing deformation rate. Rate-independent plasticity is recovered in the limit of small $\mu \ll \tau_y/\dot\gamma_0$.

Linear viscoplasticity can be generalized to account for strain hardening, by assuming that the critical stress at which flow initiates is an increasing function of the plastic strain, $\tau_y \to \tau_y(\gamma)$ in equation (4). Other generalizations may include nonlinear relationships between stress and strain rate, and the inclusion of additional variables such as temperature, or of internal variables describing the material microstructure.

Plastic instabilities and stable plastic flow Under 'normal' deformation conditions, a strain hardening viscoplastic material responds to a homogeneous driving stress in a spatially homogeneous manner. Under certain conditions, however, small perturbations of a homogeneous flow mode may become undamped, and one is dealing with a *plastic instability*. We consider linear viscoplastic flow with a generic strain dependence of the yield stress. In the plastic regime we have from equation (4)

$$\dot\gamma = \frac{\tau - \tau_y(\gamma)}{\mu}, \tag{6}$$

where τ is now understood as an externally applied shear stress which we take without loss of generality to have positive sign. One may now consider the evolution of small local perturbations $\delta\gamma$ of some homogeneous deformation mode $\gamma_0(t)$ – for instance, $\gamma_0(t) = \dot\gamma_0 t$ for a constant imposed strain rate $\dot\gamma_0$, or the response $\gamma_0(t)$ to

a stress $\tau = \dot{\tau} t$ ramped up at a constant rate. The evolution of perturbations is in either case given by

$$\delta\dot{\gamma} = -\frac{\theta(\gamma_0)}{\mu}\delta\gamma, \quad \theta = \frac{\partial\tau_y}{\partial\gamma}, \tag{7}$$

provided that the external stress is unchanged by the perturbation. Perturbations become undamped if either the tangent modulus θ or the viscoplastic coefficient μ turn negative. The first case is referred to as *strain softening*, the second as *strain rate softening* instability. This terminology can be rationalized from equation (5) for the flow stress: In case of strain softening the partial derivative $\partial\tau_f/\partial\gamma|_{\dot{\gamma}}$ and in case of strain rate softening the partial derivative $\partial\tau_f/\partial\dot{\gamma}|_{\gamma}$ become negative.

Plastic instabilities give rise to various kinds of interesting phenomena like nonlinear oscillations, travelling waves, deformation localization, patterning and chaos. An overview of these phenomena can be found elsewhere [2, 3]. Generally speaking, instability of the homogeneous deformation mode reveals the presence of internal length and time scales (for the role of internal length scales in plastic instabilities and the related problems for constitutive modelling, see, e.g. Aifantis [11, 12]; for the problem of internal time scales and the relationship between strain rate softening and Hopf bifurcations, see Hähner and Zaiser [13]).

In the context of the present paper, however, we are interested in collective phenomena during 'stable' plastic deformation. In this context it is useful to come back to the simplest plasticity model: that of a rate-independent ideally plastic material. From the point of view of plastic stability/instability, deformation of such a material is marginally stable both in the strain and strain rate softening sense, since both the hardening and viscoplastic coefficients are by definition equal to zero. Hence, fluctuations may become relevant on all scales, and it is not astonishing that different kinds of critical phenomena may be observed as soon as one approaches the yield stress. Of course, rate-independent ideal plasticity does not exist in real materials – but it is not a completely off-the-mark approximation either: If we measure stresses in units of the shear modulus G, then the characteristic hardening rates of most crystalline materials are small (typically $10^{-4} < \theta/G < 10^{-2}$). The same is true for the rate-dependent contribution to the flow stress, which is small at least in fcc and hcp metals and for deformation rates accessible in standard deformation testing. In consequence, deforming crystals can often be envisaged as slowly driven non-equilibrium systems whose internal dynamics are characterized by intermittent jumps between metastable near-equilibrium configurations of the defect microstructure: Most of the time, almost nothing is happening in most of the crystal volume, while plastic flow occurs through intermittent bursts of activity which are associated with collective rearrangements in the microstructural pattern and lead to sudden increments in strain [4, 14]. To better understand the nature of these rearrangements, it is necessary to envisage plasticity on the level of crystal dislocations.

1.2. *Crystal plasticity on the dislocation level: yield stress and depinning transition*

Dislocations and plasticity The physicist's approach towards plasticity has always focused on the elementary mechanisms of plastic flow in a material with a given

atomic structure, rather than on constitutive equations for the flow of a continuous medium. The elementary mechanism of crystallographic slip is not the rigid sliding of lattice planes above each other, but the expansion of a slipped area. The boundary of a slipped area is a one-dimensional lattice defect: a dislocation. A dislocation line is characterized globally by the slip plane and by the Burgers vector of the corresponding slip system, and locally by a unit tangent vector $\mathbf{t}$ characterizing the line direction. Depending on the angle between $\mathbf{t}$ and $\mathbf{b}$, it is conventional to distinguish edge ($\mathbf{t} \perp \mathbf{b}$), screw ($\mathbf{t} \parallel \mathbf{b}$) and mixed segments. A shear stress τ acting in the dislocation slip system creates a force per unit length on the dislocation (Peach–Koehler force, [15]). The component of this force in the dislocation glide plane (with normal vector $\mathbf{n}$) is given by

$$\mathbf{F}_{\mathrm{PK}} = \tau b[\mathbf{t} \times \mathbf{n}]. \tag{8}$$

This force perpendicular to the dislocation line acts as the driving force for dislocation glide: it moves the dislocation such as to shear the material in the direction imposed by the slip geometry and the sign of the stress τ.

The lattice around a dislocation is distorted: dislocations possess long-range stress fields. The stress field of a straight dislocation is given by

$$\tau_{\mathrm{D}}(\mathbf{r}) = \frac{Gb\Psi(\theta)}{r}, \tag{9}$$

where θ is the angle in the plane perpendicular to the dislocation, r is the vertical distance from the dislocation, and the function Ψ has zero average. The stress field of a curved dislocation can, at least outwith the immediate vicinity of the dislocation line, be considered as a superposition of stress fields of short straight segments,

$$\tau_{\mathrm{S}}(\mathbf{r}) = \frac{Gb\Phi(\theta,\phi)\mathrm{d}s}{|\mathbf{r}|^2}, \tag{10}$$

where $\mathbf{r}$ is now the vector connecting the segment to the point under consideration, $\mathrm{d}s$ is the length of the segment and Φ is another angle-dependent function whose average over the unit sphere vanishes (for explicit expressions, see [16]). The long-range stresses associated with dislocations or dislocation segments lead in the case of curved dislocations to self-interactions (which tend to keep the dislocation straight), and in general to interactions between different dislocation lines. Plasticity on the dislocation level corresponds to the collective dynamics of a system of interacting elastic lines under the action of external driving forces.

Leaving for the moment the question of dislocation creation aside (most crystalline solids contain appreciable densities of dislocations resulting from crystal growth and preparation history), a crystal will yield plastically if the applied stress is sufficient for the sustained motion of a generic lattice dislocation. In general, this motion will in turn increase the dislocation density, as the expansion of dislocation loops increases the dislocation length contained in the crystal. (The generation of dislocations *ex nihil* requires stresses which are orders of magnitude above those required to move existing dislocations; this is a process which is hardly relevant for plasticity except in extreme cases such as the deformation of dislocation-free whiskers.)

Hence, from the dislocation point of view yielding is the onset of sustained motion of a generic dislocation: Yielding is dislocation depinning. We will first consider the depinning of a single dislocation (or a hypothetical population of non-interacting dislocations), which reduces to the well-investigated problem of a single one-dimensional elastic manifold moving through a two-dimensional disordered medium. Even though this picture is not fully realistic (real dislocations *do* interact over long distances), it will be useful for introducing relevant concepts and notations of the literature on depinning transitions.

Depinning transition of a single dislocation We envisage a dislocation gliding in the $z=0$ plane. The dislocation is assumed to be on average straight and to run along the x direction. The Burgers vector is $\mathbf{b}=b\mathbf{e}_y$ (edge dislocation). A shear stress τ is applied to the considered volume element from outside and creates an external driving force acting on the dislocation. If the dislocation line is not compeletely straight, elastic interactions between different segments will create a stress that tends to straighten the dislocation; for small perturbations $y(x)$ of a straight line this stress can be written as

$$\tau_{\text{self}}(x)=\int\left[y(x)-y(x')\right]\Gamma_{\text{D}}(x-x')\mathrm{d}x', \tag{11}$$

where the stress kernel Γ_{D} decreases in space like $1/|x-x'|^3$ (for explicit expressions, see [17]). In the theory of depinning, it is usual to classify elastic kernels in terms of their long-wavelength behaviour in Fourier space. A $1/r^3$ kernel acting on a one-dimensional manifold scales like $|\mathbf{k}|^2$ with logarithmic corrections, which puts the problem into the realm of local elasticity: This is why the self-interaction of a dislocation can be represented to a good approximation by a local line tension.

In addition to its self-interaction, the dislocation interacts with other defects (atomic defects or other dislocations) which create an effective pinning force. We assume a random defect arrangement which gives rise to a spatially fluctuating internal stress field $\delta\tau(\mathbf{r})$ with zero average and short-range correlations:

$$\langle\delta\tau(\mathbf{r})\rangle=0,\quad \left\langle\delta\tau(\mathbf{r})\delta\tau(\mathbf{r}+\mathbf{r}')\right\rangle=\left\langle\delta\tau^2\right\rangle\xi_{||}\delta(x')f_\tau(y'), \tag{12}$$

where f_τ is a short-ranged correlation function of characteristic range $\xi_\perp$, and $\xi_\parallel$ and $\xi_\perp$ are correlation lengths of the fluctuating stress field in the directions parallel and perpendicular to the dislocation, respectively. The pinning defects are assumed to be immobile (quenched disorder).

Moving dislocations experience a friction force due to scattering of phonons and electrons. Since the effective mass of dislocations is generally small, their motion is under most circumstances overdamped, i.e. the velocity is proportional to the acting force. For a straight dislocation with small perturbations, the equation of motion of the dislocation line becomes

$$\frac{1}{\mu_{\text{D}}b}\partial_t y(x)=\tau+\int\left[y(x)-y(x')\right]\Gamma_{\text{D}}(x-x')\mathrm{d}x'+\delta\tau(x,y), \tag{13}$$

where μ_{D} is the dislocation drag coefficient. Equation (13) is a variant of the quenched Edwards–Wilkinson equation describing the motion of an elastic interface (elasticity mediated through the kernel Γ_{D}) through a disordered medium

(characterized by the quenched random field $\delta\tau(x, y)$) under the action of an external driving force. Since this problem has received extensive attention in the literature (see the reviews by Leschhorn *et al*. and by Fisher [18, 19], or the more recent works of Le Doussal and co-workers [20, 21]), we here only summarize the main results in dislocation language:

- Below a critical driving stress τ_c, the dislocation gets asymptotically pinned ($v = \langle \partial_t y \rangle \to 0$ for $t \to \infty$ and $\tau < \tau_c$). The magnitude of the critical stress depends on the statistical properties of the pinning field $\delta\tau$, and on the relative magnitude of the pinning and self-interactions. Practically all the metallurgical literature on the problem is devoted to evaluating this critical stress for the various types of pinning fields that may be encountered in different metals and alloys. Some classical estimates can be found in the works of Labusch, Larkin and Friedel [15, 22–24]. While the pinning strength of a given disordered microstructure is of paramount importance for applied metallurgy (dislocation pinning may determine the strength of the turbine blades in your aircraft), we will adopt a statistical physicist's stance and focus on the universal dynamical properties at the depinning transition, for which the yield stress (being a non-universal quantity anyway) is of little relevance.
- At the depinning stress τ_c, a dynamic phase transition occurs from a pinned to a moving phase. This transition is second-order-like, with the mean velocity of the dislocation – which plays the role of an order parameter – increasing like

$$v \propto (\tau - \tau_c)^{\beta} \tag{14}$$

  where β is called the *velocity exponent*. Well above the critical stress (for $\tau \gg \langle \delta\tau^2 \rangle^{1/2}$), the disorder becomes irrelevant and the dislocation velocity increases linearly with stress. This situation is schematically depicted in figure 3.
- Near the critical stress the dislocation assumes a self-affine lineshape. A self-affine curve $y(x)$ is statistically invariant under the transformation $x \to \lambda x, y \to \lambda^{\zeta} y$, where ζ is the *roughness exponent*. Scale invariance is delimited by an upper correlation length ξ which diverges as one approaches the critical stress,

$$\xi \propto |\tau - \tau_c|^{-\nu}, \tag{15}$$

  with the *correlation length exponent* ν. As a consequence of the self-affine behaviour, the mean height difference between two points along the line scales like

$$\big\langle |y(x) - y(x + l)| \big\rangle \propto l^{\zeta} f_y(l/\xi), \tag{16}$$

  where the scaling function f_y has the asymptotic properties $f_y(u) = 1$, $u \ll 1$ and $f_y(u) = u^{-\zeta}$, $u \gg 1$. Roughening of an initially straight dislocation starts on small scales, over domains of size $l \propto t^{1/z}$ where z is called the *dynamic exponent*. Near the critical stress, the transient dynamics is described by the Family–Vicsek scaling form [25]

$$\big\langle |y(x) - y(x + l)| \big\rangle = l^{\zeta} f_y\left(\frac{l}{t^{(1/z)}}\right), \tag{17}$$

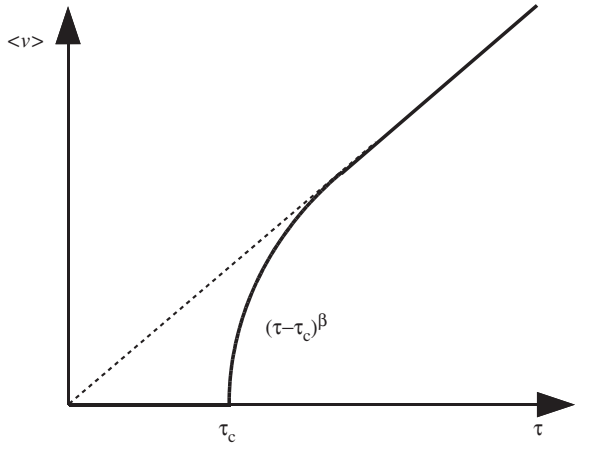

Figure 3. Stress–velocity relation for a depinning dislocation.

which is also observed in a wide class of other problems including the thermal roughening of elastic manifolds and diverse models of surface growth.

- Near the critical stress, the motion of the dislocation proceeds through intermittent *avalanches* during which segments rapidly sweep forward before they get trapped again. In the pinned phase, release of an avalanche from a trapped configuration is contingent upon a small increase in the external stress. In the moving phase, on the other hand, the system never gets completely trapped and the definition of an 'avalanche' therefore requires the introduction of a velocity threshold. In either case, the avalanches exhibit a power-law size distribution,

$$p(s) = s^{-\kappa_s} f_s(s/s_0), \tag{18}$$

where the avalanche size s corresponds to the swept area, κ_s is the *avalanche exponent*, and the scaling function f_s ($f_s(u) \to 1$ for $u \to 0$, $f_s(u) \to 0$ for $u \to \infty$) decays for large u faster than algebraically. The cut-off of the power-law distribution corresponds to an avalanche of characteristic extension ξ in the x direction, hence $s_0 \approx \xi^{1+\zeta} \propto |\tau - \tau_c|^{-\nu(1+\zeta)}$. The duration of an avalanche is related to its extension in the x direction through the dynamic exponent, $t \propto x^z$, and to its size by $t \propto s^{z/(1+\zeta)}$.

This type of behaviour is found in many physical situations where elastic manifolds move through some kind of pinning field. Examples include dislocations [17], vortex lines in superconductors, cracks [19], domain walls in ferromagnets [26], grain boundaries [27], contact lines in wetting, and sliding interfaces in friction [28]. In the following paragraph, we give scaling relations as well as a 'catalogue' of critical exponents for different dimensionality of the interface and range of its elastic self-interaction.

Critical exponents and scaling relations for depinning transitions We consider a d-dimensional interface moving in $d+1$ dimensions (for a dislocation moving on

Table 1. Critical exponents for interface depinning as a function of the parameters d and a; functional renormalization results (FRG, expansion in $\varepsilon = d_c - d$) after Le Doussal *et al.* [21]; mean-field results after [26].

	d	a	$FRG\mathcal{O}(\varepsilon)$	$FRG\ \mathcal{O}(\varepsilon^2)$	Simulation
Roughness	1	2	1.00	1.43	1.25 ± 0.05 [18]
ζ	2	2	0.66	0.86	0.75 ± 0.02 [18]
	3	2	0.33	0.38	0.34 ± 0.01 [18]
	1	1	0.33	0.47	0.34 ± 0.02 [29]
		MF		0	
Correlation length	1	2	0.75	0.98	1.00 ± 0.05 [30]
ν	2	2	0.67	0.77	0.77 ± 0.04 [31]
	3	2	0.58	0.61	
	1	1	1.33	1.58	1.52 ± 0.02 [29]
		MF		$2/d$	
Velocity	1	2	0.67	0.31	0.25 ± 0.03 [18]
β	2	2	0.78	0.62	0.64 ± 0.02 [18]
	3	2	0.89	0.85	0.84 ± 0.01 [18]
	1	1	0.78	0.59	0.68 ± 0.06 [29]
		MF		1	

its glide plane, $d = 1$). We exclude overhangs, so the interface can be characterized by a single-valued function. The elastic self-interaction of the interface is characterized by an elastic kernel $\Gamma(\mathbf{r})$ ($\mathbb{R} \in {}^{d}$) whose Fourier transform scales like $|\mathbf{k}|^a$ for $|\mathbf{k}| \to 0$, i.e. in real space it decays like $|\mathbf{r}|^{-d-a}$, or possibly faster for $a = 2$. The interface moves under the action of a generalized force (or stress) τ across a time-independent random force field of zero average and with short-range spatial correlations.

The main characteristics of the dynamics have been discussed in the previous section for the special case of an isolated dislocation. Numerical values for the velocity, correlation length and roughness exponents are compiled in table 1, including results from functional renormalization (Le Doussal *et al.* [21]) and from simulations (references cited). We also include values for the mean-field case which become valid above the critical dimension $d_c = 2a$ [19, 26].

In the following we compile some scaling relations that may be useful for the later discussion. All relations will be motivated by intuitive scaling arguments; for a rigorous derivation the reader is referred to the literature.

- A relation between the dynamic and velocity exponents is found by noting that the mean velocity of the interface is governed by the largest jumps, during which segments of linear extension ξ move over distances ξ^{ζ}. The time it takes the interface to reach an (almost) pinned configuration is $t \propto \xi^{z}$, and $\xi \propto (\tau - \tau_c)^{-\nu}$ in the moving phase. Hence the velocity exponent obeys the scaling relation

$$\beta = \nu(z - \zeta). \tag{19}$$

- The avalanche exponent can be related to other exponents by considering the average susceptibility which is proportional to the mean avalanche size, $\chi = \partial\langle y\rangle/\partial\tau \propto \langle s\rangle$. On the one hand, $\chi \propto \xi^{\zeta}/\xi^{1/\nu}$, hence

$$\chi \propto (\tau_c - \tau)^{-(1+\nu\zeta)}. \tag{20}$$

  On the other hand, the mean avalanche size is

$$\langle s\rangle \propto s_0^{2-\kappa}, \quad s_0 \propto (\tau_c - \tau)^{-\nu(d+\zeta)}. \tag{21}$$

  Combining these relations, we find the exponent relation [26, 32]

$$\kappa = 2 - \frac{1+\zeta\nu}{\nu(d+\zeta)}. \tag{22}$$

- Additional relations can be found for the relation between size and duration of an avalanche, and for the relaxation of the mean velocity near the critical stress. The size of an avalanche of linear dimension x is $s = x^{d+\zeta}$, and the corresponding time scale is $t = x^z$, hence

$$t \propto s^{z/(d+\zeta)}. \tag{23}$$

  For the velocity relaxation near the critical point we find the scaling $v \propto x^{\zeta-z}$ and with $t \propto x^z$ we get

$$v \propto t^{2/z-1} = t^{\beta/(\nu z)}. \tag{24}$$

In the following these exponents and scaling relations will appear in different contexts. In all of these the mean position of the 'interface' corresponds to a strain-like variable (for instance, the mean distance $\langle y\rangle$ travelled by a dislocation corresponds, for a hypothetical ensemble of non-interacting dislocations of density ρ, to the macroscopic strain $\gamma = \rho b\langle y\rangle$). The word 'interface' should be taken with a grain of salt: whereas a single dislocation clearly is an interface between a slipped and a non-slipped region, and a dislocation wall is an interface between two regions of different lattice orientation, the intuitive notion of an interface becomes much more spurious if one is dealing with a dislocation procession or pile-up. In section 3 we will even encounter a model where the 'interface' coordinates are the Cartesian coordinates of a volume element in the deforming crystal, and the direction into which this interface is 'moving' corresponds to the local shear strain. The scaling relations and exponents characterizing the dynamics are unaffected by such semantic subtleties.

2. Experimental investigation of fluctuation phenomena in plastic flow

2.1. *Acoustic emission measurements*

2.1.1. Experimental methodology. As dislocations move during plastic deformation, they lose energy to the phonon and electron systems in the crystal. In many situations, the resulting drag force is so large that dislocation motion effectively proceeds in an over-damped manner. If dislocation motions are sufficiently rapid, the energy loss cannot be exclusively envisaged in terms of dissipation and heat

generation, but part of the energy is emitted in the form of travelling acoustic waves which can be detected as an acoustic emission signal. Therefore, acoustic emission recordings may be used as a tool for monitoring dislocation activity during plastic deformation.

A major problem in the interpretation of acoustic emission signals is, however, to establish the relation between the observed voltage record and the underlying dislocation processes. The transmission function between the acoustic source and the recorded signal is in general very complicated and, more importantly, the source characteristics themselves have to be understood and related to the amplitude of the emitted acoustic wave. Most investigations of source characteristics envisage the expansion of a compact dislocation loop [33, 34], or a procession of loops emitted from a common source [35]. Generally it is found that the amplitude of the emitted acoustic wave is proportional to the velocity v of the expanding loop: hence the acoustic power, which is the square of the amplitude, is proportional to v^2. In general, however, acoustic emission may be due to the simultaneous motion of many dislocations or dislocation segments, rather than the expansion of a single loop. Rouby and co-workers [33, 34] analyse the uncorrelated superposition of events coming from different sources as a paradigm for a 'continuous' AE signal, as well as a sequence of closely correlated events from one source which they use as a paradigm for a 'discrete' AE burst. In reality, the situation may be more complicated since the AE signal during a deformation avalanche may be produced by temporally correlated dislocation motions at different locations which, owing to the long-range interactions characteristic of dislocation systems, may be distributed according to complicated spatial patterns with long-range correlations (see section 3.2). For a burst during which N dislocation segments of characteristic length l move collectively at locations close to each other and with a constant velocity v, the peak acoustic emission amplitude is [36]

$$A = \frac{KNl\langle v\rangle}{r} \propto K\frac{l}{r}\dot{\gamma}. \tag{25}$$

In this equation, r is understood as the distance from the source to the acoustic transducer and K is a constant containing material properties (sound velocities) as well as transducer properties. It is seen from equation (25) that for burstlike emission the acoustic emission amplitude is essentially proportional to the instantaneous strain rate.

2.1.2. Acoustic emission in single- and polycrystals of ice. Very systematic and comprehensive investigations of the statistics of acoustic emission bursts have been performed by Weiss and co-workers on ice single- and polycrystals [6, 7, 36–41]. Ice may be considered an ideal 'model material' for AE studies of crystal plasticity for several reasons [38]: (i) Even at comparatively low stresses and temperatures close to the melting point, plastic flow of ice proceeds by glide of dislocations (in most other materials, at high temperatures and low stresses diffusional deformation mechanisms become predominant). (ii) Single crystals of hexagonal ice I_h exhibit very pronounced plastic anisotropy, as deformation occurs essentially by glide on basal planes. As a consequence, deformation by dislocation glide on a single slip system is robust in comparison with metals, where single slip is confined to very

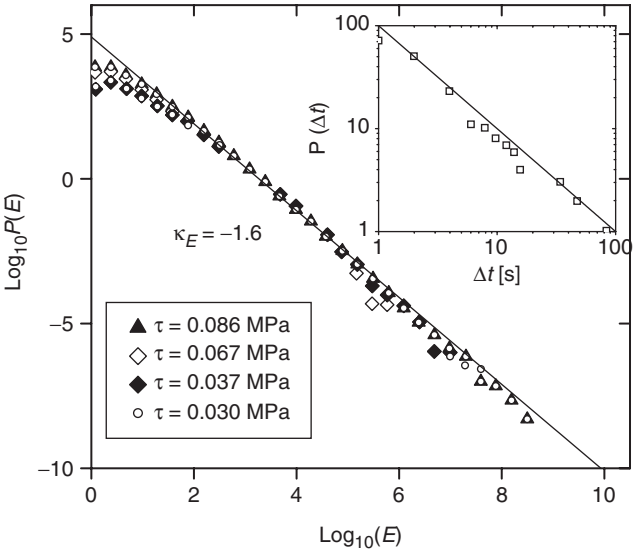

Figure 4. Energy distribution of AE events recorded during creep deformation of ice single crystals; temperature $T = 263$ K, resolved shear stresses on the basal plane as indicated in the inset, after Miguel *et al*. [6]; insert: cumulative distribution of time intervals between AE events recorded during creep of an ice single crystal at a resolved shear stress of 0.58 MPa, after Weiss *et al*. [37].

small strains. (iii) Transparency of the samples allows us to verify that AE activity is not due to microcracking. (iv) Excellent acoustic coupling can be achieved by freezing the transducers onto the sample surface.

In their studies, Weiss and co-workers focus on creep at elevated temperatures ($\sim -10^{\circ}$C) and low stresses ($\sim$1 MPa). They observe an intermittent acoustic emission signal composed of discrete AE bursts and systematically investigate the statistics of the bursts and their temporal and spatial correlations.

Avalanche statistics In their investigations, Weiss *et al*. characterize the burstlike AE signal from ice single- and polycrystals both in terms of the peak amplitudes $A = \max[A(t)]$ and in terms of the acoustic energy $E = \int_{\mathcal{B}} A^2(t)\mathrm{d}t$ where $\mathcal{B}$ denotes a compact interval over which the AE intensity exceeds a given threshold (of course, one has to check whether the statistics is robust against changes of the threshold value). For single crystals, the observations indicate scale-free distributions of burst amplitudes and energies (see figure 4),

$$p(E) \propto E^{-\kappa_E}, \quad p(A) \propto A^{-\kappa_A}, \tag{26}$$

with exponents $\kappa_E \approx 1.6$ and $\kappa_A \approx 2.0$ that are approximately independent on stress, strain, and temperature [40]. The distribution of time intervals Δt between AE events was also investigated. A cumulative distribution $P(\Delta t) \propto \Delta t^{-1}$ (i.e. $p(\Delta t) \propto \Delta t^{-2}$ for the non-cumulative distribution) was reported by Weiss and co-workers in [37] (insert in figure 4).

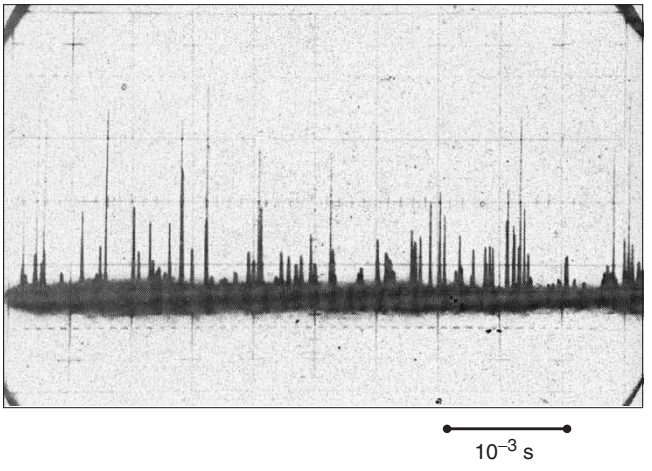

Figure 5. Acoustic emission signal (amplitude vs. time) recorded during compression testing of an Al polycrystal; after Imanaka *et al*. [42].

Investigations on polycrystals show an altogether more complex picture [40, 41]. Unlike single crystals where the amplitude and energy distributions of AE bursts are scale-free over the entire accessible amplitude/energy range, the burst amplitudes and energies in AE signals of polycrystals have upper limits which increase with increasing grain size. Furthermore, the avalanche exponents are reduced in comparison with single crystals ($\kappa_A \approx 1.35$ in polycrystals). It has been inferred from these observations that grain boundaries may act as efficient barriers to the propagation of slip avalanches. The existence of such barriers may lead to substantial stress concentrations (intergranular stresses), and it has been suggested that such overstresses may explain the observed decrease in the avalanche exponent, as they may help small avalanches to coalesce into larger ones, up to a scale governed by the grain size [40, 41]. Even more complicated behaviour has been observed in polycrystals with a bimodal grain size distribution containing a few very large grains: In these polycrystals, a single-crystal exponent $\kappa_A \approx 2$ at small avalanche sizes and a polycrystal exponent $\kappa_A \approx 1.35$ at larger sizes have been observed simultaneously.

Spatial patterns and space–time correlation of deformation avalanches By using multiple acoustic transducers, Weiss and Marsan [7] investigated the spatial location of acoustic emission 'events' in ice single crystals. By recording the arrival times of the acoustic signal at different locations and using spatial triangulation, they were able to locate the points of origin of the AE signals emanating from large deformation events with an accuracy of about 400 μm, limited by the time resolution of the recording device. They used the correlation integral method to analyse the spatial pattern of the points of origin of the AE signals (i.e. the points where deformation avalanches have initiated). Their results indicate a self-similar pattern with a correlation dimension of $D_F \approx 2.5$. The observed scaling regime extends over about 1.5 orders of magnitude; it is limited from above by the specimen size and from below by the spatial resolution of the recording technique.

The same investigation also revealed a space–time coupling in the avalanche dynamics: Avalanches that are close in the sequence of events tend also to be closer than average in space. This observation complements studies of the temporal correlation of deformation events: An analysis of the temporal correlation function revealed temporal clustering of deformation events [38] and a more detailed investigation showed an enhanced 'aftershock activity' after big deformation avalanches, with an average number N_A of aftershocks that was found to be proportional to a power of the avalanche amplitude, $N_A \propto A^{0.6}$ [39]. These findings provide evidence for the existence of a coupling between different deformation events that leads to their clustering both in space and in time.

2.1.3. Acoustic emission in metals and alloys. Acoustic emission studies have been reported on various pure metals and alloys [33, 34, 42–44]. The observed AE signals include both discrete bursts and continuous noise, sometimes occurring simultaneously in the form of discrete spikes with a continuous background [43]. Unfortunately, in the older literature there exist few statistical investigations of burst characteristics, e.g. in terms of amplitude or energy distributions. Instead, the traditional paradigm of plastic flow as a more or less continuous process led many researchers to focus on the continuous background from which the discontinuous bursts were seen as a kind of pathological exception. For instance, Kiesewetter and Schiller [43] report discrete dislocation bursts superimposed on a continuous background signal but attribute only the continuous background to dislocation motion. In line with this practice, most AE studies attempt to establish relations between plastic flow characteristics and parameters of the AE signal that are averaged over the fluctuations of the dynamics, such as the mean intensity or, in case of burst-like signals, the mean burst rate.

Very recently, Richeton *et al*. have provided a statistical investigation of the acoustic emission bursts that are generically observed in deformation of hexagonally close-packed (hcp) metals and alloys [45]. This investigation demonstrates that AE bursts in single crystals of Cd and ZnAl exhibit scale-free energy distributions with exponents $\kappa_E \approx 1.5$ that are very similar to those observed in ice single crystals. Also other findings, such as the observation of temporal correlations between AE bursts, were analogous. This result is remarkable in several respects: (i) The experiments on hcp single crystals were conducted in tension at constant crosshead velocity, which is a quite different loading mode from the constant-stress creep conditions under which the ice results were obtained. (ii) The same scale-free distribution of burst energies was found in hardening stage I (deformation by dislocation glide on a single slip system), in hardening stage II (preferential deformation on a single slip system, but strong forest hardening because of additional dislocation activity on secondary slip systems), and for crystal orientations where deformation proceeds mainly by twinning. These findings demonstrate a remarkable robustness of the scale-free behaviour of AE signals in plastically deforming crystals and indicate that intermittent 'crackling' noise [46] may be a universal signature of deformation by crystallographic shear (slip or twinning).

2.2. *Deformation-induced surface patterns*

Plastic deformation leads to characteristic surface phenomena which can be used to monitor the flow process and gain information on plastic flow patterns. Along the lines of intersection between the active slip planes and the surface, moving dislocations leave behind them atomic-scale surface steps ('slip lines') which can be considered as records of the dislocation movements which have produced them. Characterization of plastic deformation using surface micrographs is an 'old' experimental technique which dates back to the 1950s. With the advent of transmission electron microscopy, surface-based techniques fell somewhat out of favour, since dislocation motion near free surfaces is inevitably affected by surface effects – for instance, the presence of a free surface modifies the stress field such that dislocations near surfaces experience image forces and may annihilate at the surface, leading to the formation of a soft dislocation-depleted surface layer with a width of a few (bulk) dislocation spacings. The problem of surface-induced artefacts is most significant if one wants to study small-scale features (arrangement and motions of individual dislocations or dislocation groups) but may be less critical if one is looking for scale-free features.

As far as scale-free patterns in plastic flow of solids are concerned, surface-based techniques have one distinct advantage: Surface investigations give the possibility to characterize deformation-induced surface patterns from the atomic up to the macroscopic scale in terms of a single type of experimental information (surface height, positions of surface steps). Bulk techniques operating on different scales, on the other hand, have to cope with the difficulty that the different techniques (e.g. transmission electron microscopy and X-ray topography) yield qualitatively different types of information. Data obtained by different techniques can therefore not be simply stitched together to yield a comprehensive multiscale characterization.

In view of the availability of experimental techniques covering features from the atomic to the macroscale, and the simplicity of compiling information from different scale regimes into a comprehensive picture, surface techniques seem particularly suited to monitor the multiscale organization of plastic deformation through different stages of the deformation process and to detect scaling laws and scale-free features. This may be done by looking at the distribution of slip lines on the surface, which give local information on the deformation process in terms of the positions where individual dislocations have left the surface producing units of slip, or by looking at surface profiles which yield the corresponding integral information about the global slip pattern.

2.2.1. Slip-line patterns. Slip lines emerging under single-slip conditions form striated patterns of parallel lines (figure 6), and it was suggested already in the 1980s that the points of intersection of the slip lines with a line drawn normal to them might form some kind of randomized Cantor set. This proposition was followed up by Sprusil and Hnilica [47] and Kleiser and Bocek [48]. Sprusil and Hnilica [47] tried to deduce a fractal dimension by determining the mean slip line spacing from micrographs of different magnification. This is methodologically spurious, as discussed in [10] in relation with the fractal analysis of dislocation cell patterns. Kleiser and Bocek [48], on the other hand, provided a systematic

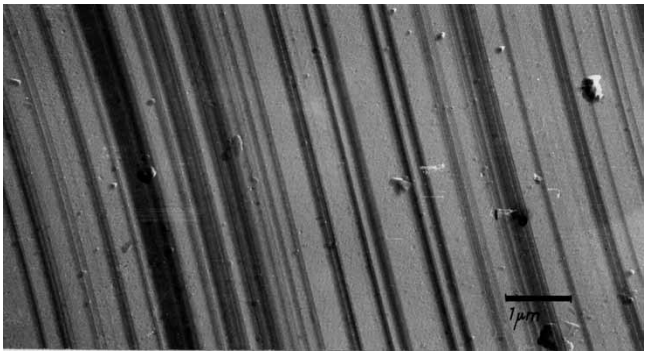

Figure 6. Slip lines on the surface of a Cu-30 at% Zn single crystal deformed in tension at 77 K to a strain of 19.4%. Courtesy of H. Neuhäuser.

investigation using various techniques (gap width distribution, box counting, and correlation integral) to determine the fractal dimension of slip line patterns. Their findings may be summarized as follows:

- Slip lines on the surface of a Cu single crystal that were generated within a narrow strain interval ($0.59 < \gamma < 0.69$) exhibit a statistically self-similar pattern over a range of scales between typically 0.06 and 2 μm. The set of intersection points with a normal line has a fractal dimension of $D \approx 0.4-0.7$, depending on the method used.
- Slip lines accumulating over a larger strain interval from the beginning of deformation form a more or less homogeneous pattern without clear evidence of self-similar behaviour.

These findings indicate long-range correlated fluctuations in the flow process which, however, persist only over limited intervals of time (or strain). The investigations of Kleiser and Bocek, and Sprusil and Hnilica, were based upon the analysis of optical surface micrographs dating from the 1950s and 1960s. A problem with these micrographs is that they do not allow us to quantitatively resolve the height of the slip steps, i.e. the number of dislocations that have exited the crystal along a given slip line or, equivalently, the local strain concentration. The observed long-range correlations in the slip-line pattern can therefore not be directly translated into correlations in the strain pattern. A semi-quantitative analysis was provided by Kleiser and Bocek who estimated the slip step height from the width of slip lines visible on surface micrographs and used this to 'weight' the lines. Fractal dimensions of the resulting weighted patterns were somewhat higher than those of slip-line patterns with all visible lines given equal weight. A more quantitative analysis could nowadays be provided by using atomic-resolution AFM to determine the height and spacing of surface steps, but this remains still to be done.

2.2.2. Slip-line kinematography. By *in situ* optical observation of the surface of a plastically deforming crystal (so-called slip-line kinematography), it is possible to gain information about the dynamics of plastic flow. An overview of experimental

methods can be found in the review by Neuhäuser [49]. Because of the necessity of keeping in focus a small surface window which is imaged with high magnification, the technique is not suited for studying the evolution of large-scale deformation patterns, but it can give useful information about the temporal evolution of slip lines or slip-line clusters (slip bands).

Clustering of slip is pronounced in alloys exhibiting so-called planar slip where dislocations tend to move in large processions (pile-ups). In this case, one is dealing with the dynamics of linear or almost linear dislocation arrays, rather than individual dislocations. Scale-free behaviour has been observed in the growth kinetics of surface steps, where the growth rate has been found to decay in inverse proportion with the time elapsed from the onset of step growth (figure 7, [50]).

For a moving pile-up consisting of roughly equally spaced dislocations, the slip step growth rate is proportional to the pile-up velocity. Since often only a small number of slip steps are growing at a time [49], one may therefore attempt to relate the observed time dependence of slip step growth to the velocity relaxation of a single pile-up. The double-logarithmic plot in figure 7 indicates relaxation of the growth rate (the pile-up velocity) according to $v \propto t^{-1\pm0.1}$ over six decades.

According to the relations given in the introduction, a planar dislocation array in a three-dimensional crystal falls into the class $d = 2, a = 1$, i.e. the depinning transition of such arrays exhibits mean-field behaviour. For the velocity relaxation near the critical point one then expects according to equation (24) and table 1 an exponent $\beta/(\nu z) = 1$, which is in line with the experimental data. The length of the scaling regime may be taken as an indication that driving of the dislocation arrays occurs at stresses very close to the critical one.

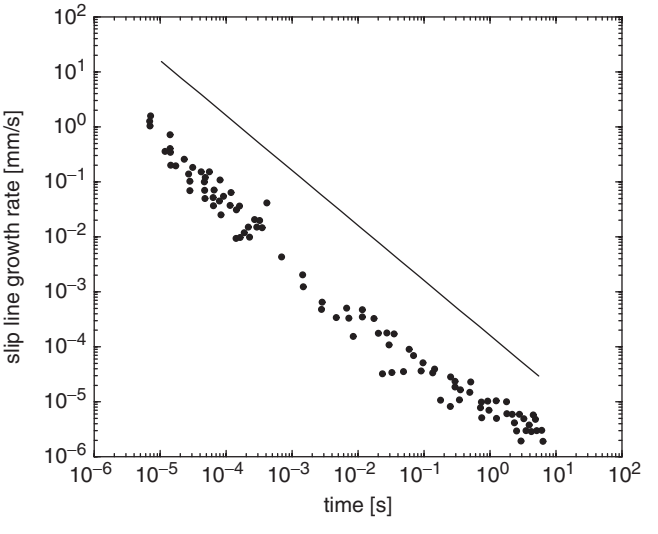

Figure 7. Growth rate of slip steps on the surface of Cu-30 at% Zn deformed at room temperature as a function of the time passed after growth has started; after [50]. The line is a power law with exponent −1.

2.2.3. Surface roughening in single- and polycrystals. Long-range correlations in the pattern of surface steps can be detected indirectly through analysis of surface profiles, even if the experimental resolution is not sufficient to resolve individual surface steps. The relation between one-dimensional surface profiles evolving from an initially smooth surface, and the plastic distortion at the surface, is straightforward: If we use a local coordinate system such that the x direction corresponds to the profile direction and the y direction is normal to the average direction of the deformed surface, then for small deformations the derivative $y_x = \partial y/\partial x$ of the profile $y(x)$ is related to the component $\epsilon^{\mathrm{p}}_{yx}$ of the plastic strain tensor by

$$\partial y/\partial x = \epsilon^{\mathrm{p}}_{yx}(\mathbf{r}) - \langle \epsilon^{\mathrm{p}}_{yx} \rangle =: \delta\epsilon^{\mathrm{p}}_{yx}(\mathbf{r}). \tag{27}$$

By looking at an appropriately oriented surface and under single-slip conditions, this can be directly translated into the shear strain fluctuation $\delta\gamma$.

Correlations in the plastic strain pattern can therefore be detected by surface profile analysis. In particular, if the strain fluctuations $\delta\epsilon^{\mathrm{p}}_{yx}(\mathbf{r})$ exhibit power-law correlations this may lead to the emergence of self-affine surface profiles with roughness exponent $\zeta > 0.5$ [8], as discussed below.

Self-affine surface morphology Several recent investigations have been devoted to self-affine scaling of the surfaces of plastically deformed metals. Zaiser *et al.* [8] applied a combination of atomic force microscopy (AFM) and scanning white-light interferometry (SWLI) to quantitatively characterize the surface of Cu polycrystals over a range of scales between 10 nm and 2 mm. Cu polycrystals of 99.9% nominal purity were plastically deformed at room temperature, and two-dimensional surface maps were determined at various degrees of deformation up to an engineering strain of 23% (tensile stress 215 MPa). The sequence of surface investigations was ended at the onset of macroscopic deformation localization (necking).

Multiple one-dimensional profiles were obtained from the surface maps in the directions both parallel and normal to the tensile axis. Two typical AFM and SWLI profiles are shown in figure 8. Roughness exponents were obtained by plotting mean height differences $\langle |y(x) - y(x+L)| \rangle$ vs. the separation distance L as shown in figure 9. Typical double-logarithmic plots exhibit linear scaling regimes extending between 0.05 and 5 μm for the AFM and between 0.5 and 50 μm for the SWLI profiles. The upper end of the SWLI scaling regime (the upper correlation length) was found to be strain-independent; it coincides with the mean grain size of the polycrystalline aggregate. Roughness exponents deduced from the slope of the scaling regimes were similar for AFM and SWLI profiles, indicating continuous scaling over almost four orders of magnitude. The exponents were checked by also applying a wavelet analysis method proposed by Simonsen *et al.* [51] to the surface profiles. Both techniques revealed a roughness exponent decreasing from an initial value close to unity, during a strain interval of about 5%, towards an asymptotic value of $\zeta \approx 0.75$. Surface profiles taken in the directions normal and parallel to the tensile axis were found to yield similar exponents.

Self-affine scaling of deformed polycrystal surfaces is also evident from the probability distributions of surface height differences. Distributions $p_L(\Delta y)$ of height differences $\Delta y := y(x) - y(x+L)$ can be collapsed by re-scaling $p_L(\Delta y) = p_{L'}((L/L')^{\zeta}\Delta y)$ with a roughness exponent $\zeta \approx 0.75$ (figure 10).

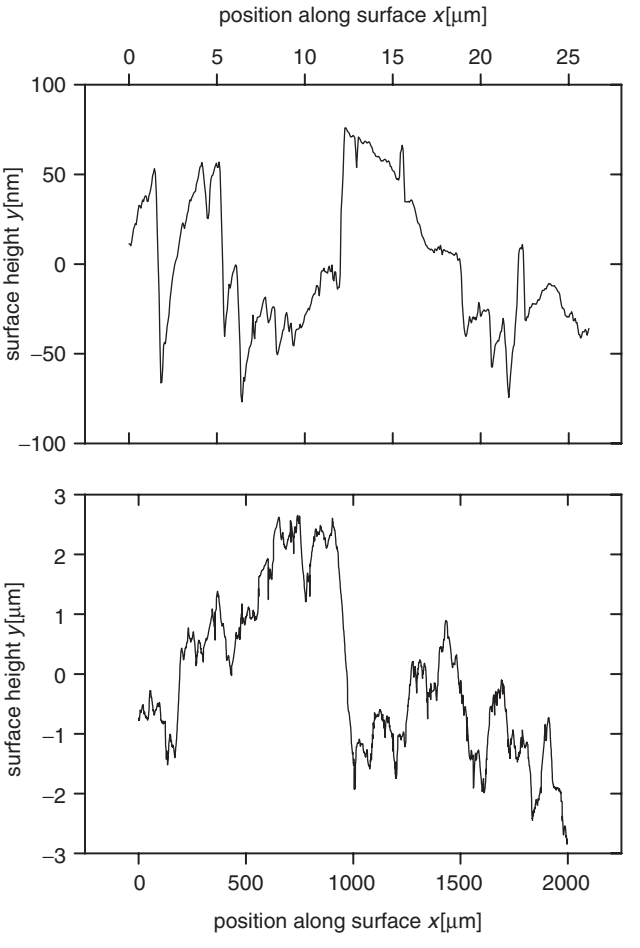

Figure 8. Surface profiles of a Cu polycrystal taken at $\epsilon = 9.6\%$; top: AFM profile; bottom: SWLI profile; the x direction is parallel to the direction of the tensile axis; roughness plots corresponding to these profiles are shown in figure 9.

The evolution of self-affine surface roughness was also studied on KCl single crystals deformed in compression [52]. Alkali halides offer the advantage that very smooth initial surfaces can be produced by cleavage. Deformation experiments on [100]-oriented crystals revealed a typical three-stage hardening curve where deformation at small strains (Stage I) proceeds in single slip with a comparatively low hardening rate, whereas at higher strains multiple slip systems become active and the strain hardening coefficient increases (Stage II, see figure 11). Surface characterization was done throughout these two hardening regimes using SWLI. Profiles taken in Stage I (figure 12, left), did not show any limits to the scaling regime below the profile length of 1.5 mm. The roughness exponent $\zeta \approx 0.65$ determined from the profiles is somewhat lower than what is observed in polycrystals and does not depend appreciably on strain. Roughness exponents ζ_q were also

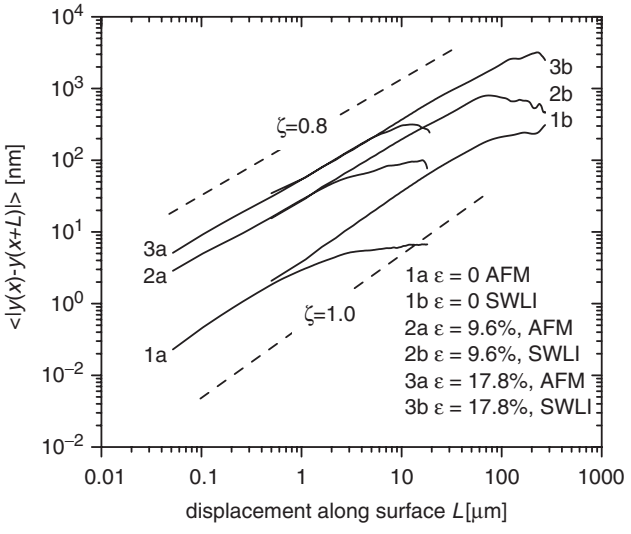

Figure 9. Roughness plots (mean height difference vs. distance along profile) for AFM and SWLI profiles obtained from the as-polished surface and after deformation to strains of 9.6 and 17.8%; the profiles for $\epsilon = 9.6\%$ are shown in figure 8.

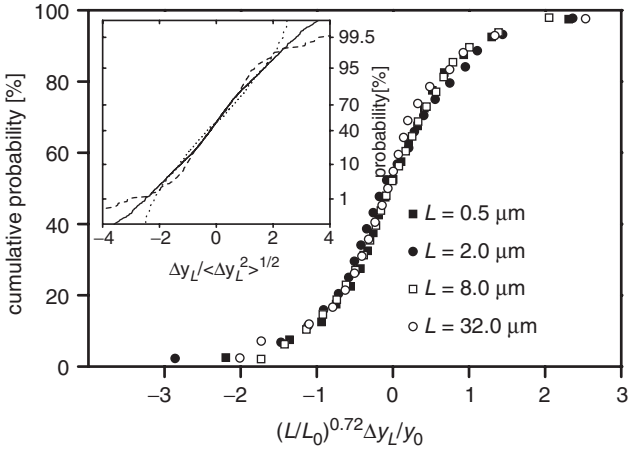

Figure 10. Scaling collapse of height difference distributions obtained from AFM and SWLI profiles of Cu polycrystal surfaces ($\epsilon = 9.6\%$); insert: distributions normalized to unit variance for $L = 40$ nm (dashed line), $L = 5\,\mu$m (full line) and $L = 160\,\mu$m (dotted line).

determined from higher-order correlation functions scaling like $\langle |h(x) - h(x+L)|^q \rangle^{1/q} \propto L^{\zeta_q}$. As expected for self-affine scaling, exponents $\zeta_q, 1 \leq q \leq 4$, were found to be approximately independent of the order q of the correlation function.

In Stage II, on the other hand (figure 12, right), the profiles have a more complex structure with a local roughness exponent $\zeta \approx 0.7$ on small scales which on larger scales possibly crosses over to an exponent of about $\zeta \approx 0.5$. At the same time, the roughening of the surface accelerates markedly (open data points in figure 11).

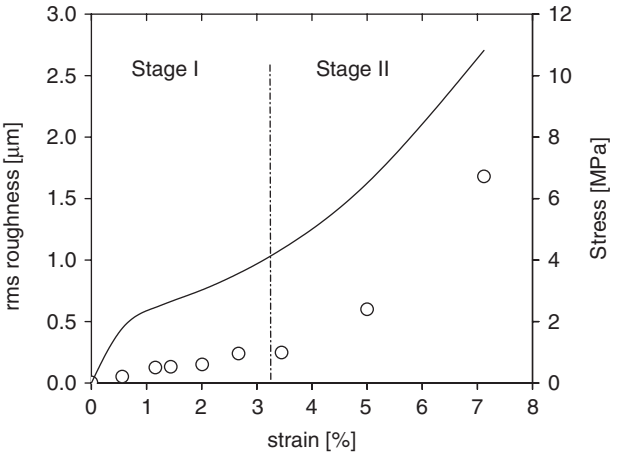

Figure 11. Stress–strain curve and rms surface roughness of a KCl single crystal deformed in compression at room temperature in [100] orientation; full line: stress–strain curve (compressive stress vs. engineering strain), open circles: rms surface roughness as determined from four profiles with length 1.5 mm.

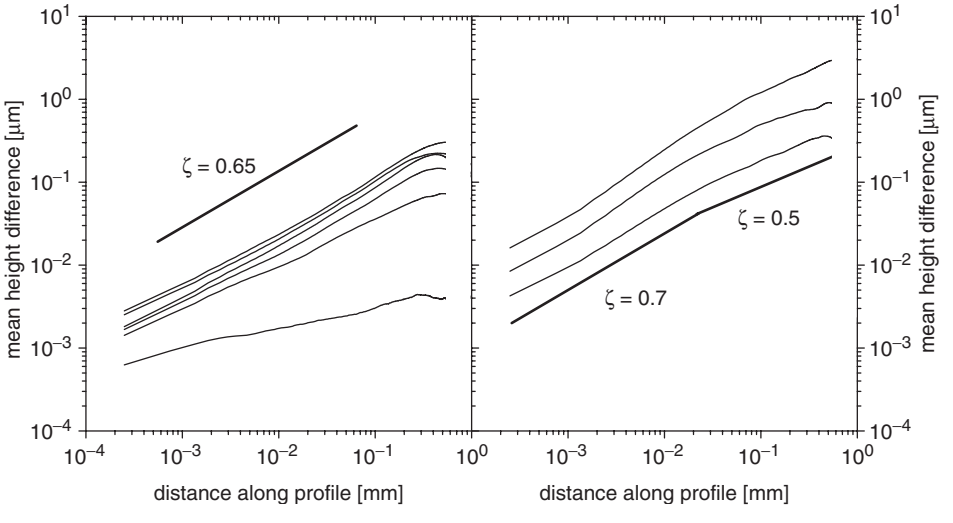

Figure 12. Local roughening of the surface of a KCl single crystal as determined by SWLI (mean height difference vs. distance along profile); left: deformation in Stage I; strains 0%, 0.56%, 1.16%, 1.44%, 2.01% and 2.67%; right: deformation in Stage II; strains 3.45%, 5.00% and 7.12%.

The self-affine scaling of surface profiles $y(x)$ observed in Cu polycrystals and after Stage I-deformation of KCl single crystals implies that the underlying stochastic process $\delta\epsilon^{\mathrm{p}}_{yx} = \partial y/\partial x - \langle \partial y/\partial x \rangle$ has long-range spatial correlations along the direction of the profile:

$$\left\langle \delta\epsilon^{\mathrm{p}}_{yx}(x)\delta\epsilon^{\mathrm{p}}_{yx}(x') \right\rangle \propto \left|x - x'\right|^{2\zeta-2} \approx \left|x - x'\right|^{-0.3\ldots-0.6}. \tag{28}$$

Provided that the plastic strain itself has the characteristics of a point process (i.e. if it is comprised of discrete and localized events), this power-law decay of the correlation function implies a correlation dimension of $D \approx 0.5$ for the distribution of such events along the line of the profile, and of $D \approx 2.5$ in three-dimensional space. This appears to be in line with the observations of Kleiser and Bocek on slip-line patterns, and with those of Weiss and Marsan on the spatial distribution of slip events [7, 48].

Dynamics of surface roughening In a large class of problems including the thermal roughening of elastic manifolds, the dynamic roughening of an elastic interface driven through a random medium, and diverse models of surface growth, the roughening dynamics can be described by the Family–Vicsek scaling, equation (17). In this case, roughening starts locally, over domains of size $\xi \propto t^{1/z}$ where z is the dynamic exponent. The correlation length ξ grows in time until it hits the system size, whereas the magnitude of the roughness on scales below the correlation length remains constant in time.

The existing investigations of deformed single- and polycrystal surfaces, however, indicate a different growth kinetics, which may be more appropriately described by the concept of anomalous scaling [53, 54]. For anomalous scaling, the local roughening is described by

$$\left\langle \left| y(x) - y(x+L) \right| \right\rangle = t^{\delta} L^{\zeta_{\mathrm{loc}}} f_y\left(\frac{L}{t^{(1/z)}}\right), \tag{29}$$

and the global roughness of the surface grows like $t^{\zeta/z}$ where ζ, ζ_{loc}, and δ are related through $\delta = (\zeta - \zeta_{\mathrm{loc}})/z$.

In their investigations on Cu polycrystals, Zaiser *et al.* found the self-affine scaling regime to be delimited by a strain-independent upper correlation length of the order of magnitude of the grain size, indicating that the correlation length may be an intrinsic material property (the grain size) rather than being governed by the dynamics of the roughening process. This idea was corroborated by Wouters *et al.* [55] who used confocal microscopy to investigate the surface morphology of polycrystalline Al-Mg alloys of different grain size. On scales below the grain size, they observe self-affine scaling with Hurst exponents $\zeta \sim 0.85$–0.9 slightly above those reported by Zaiser *et al.*, whereas above this scale they find a scale-independent value of the rms surface roughness. In the framework of anomalous scaling, equation (29), this can be formally expressed by setting $z \to \infty$ while keeping δ finite.

From the data of Wouters *et al.* [55], one deduces a growth exponent $\delta \approx 0.8$ (figure 13). Curves pertaining to different grain sizes L_G can be collapsed by re-scaling the surface height in proportion with L_G (insert in figure 13). Measurements on KCl single crystals reveal during Stage I a similar growth exponent $\delta \approx 0.8$, whereas during Stage II the growth exponent is somewhat larger ($\delta \approx 1$–1.5).

2.3. *Deformation of micron-size samples*

The heterogeneous and intermittent nature of plastic flow on microscopic and mesoscopic scales is not readily apparent in deformation experiments on macroscopic crystals where, on scales above the fluctuation correlation length, the incoherent superposition of deformation events from different parts of the specimen leads to

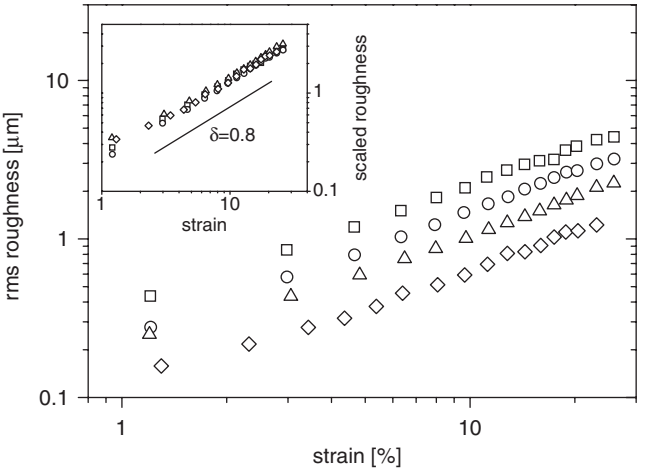

Figure 13. Anomalous surface roughening of polycrystalline Al-Mg, grain sizes $L_G = 90.1\,\mu m$ (squares), $68.1\,\mu m$ (circles), $44.9\,\mu m$ (up triangles), $30.8\,\mu m$ (down triangles); insert: scaling collapse obtained by scaling the surface width in proportion with L_G; after Wouters *et al.* [55].

a more or less smooth stress vs. strain, or strain rate vs. time, signals. Because of this, the avalanche-like character of deformation on smaller scales is not usually evident from the recordings of standard tensile or compressive tests.

Recently, however, advances in machining have allowed Dimiduk and co-workers to prepare compressive specimens with diameters down to about 1 μm (for a discussion of specimen preparation methodology, see [56]). They performed compression tests on ultra-small monocrystalline specimens of pure Ni [57–59] as well as Ni-base superalloys [56, 57] and the Ni_3Al intermetallic. Testing was carried out in a standard nanoindentation system with a flat indentation tip acting as a compression platen. Compression was performed in a particular type of load control, where the load is increased as long as the total (elastic + plastic) deformation of the specimen falls below a target value which increases linearly in time, and is kept constant otherwise. This driving mode makes it possible to directly observe large slip avalanches, which in a displacement-controlled test would be stopped by the load drop that goes along with a sudden increase in strain. From a theoretical point of view, it may be noted that this loading mode closely resembles the 'quasi-static driving' often applied in cellular automaton simulations of systems with intermittent avalanche dynamics (for examples, see sections 3.1 and 3.2): the load applied to the system is slowly increased as long as the activity of the system is zero, and is held constant during an avalanche. Stress vs. time and displacement vs. time curves resulting from such tests are shown in figure 14. It is seen that the displacement (i.e. the plastic strain) increases in discrete steps; each strain step is followed by a stress plateau which lasts until the actual strain of the specimen is matched by the 'target strain' which increases linearly in time.

In microtesting experiments carried out on specimens initially oriented for single slip, deformation was found to proceed in simple shear on a single active slip system

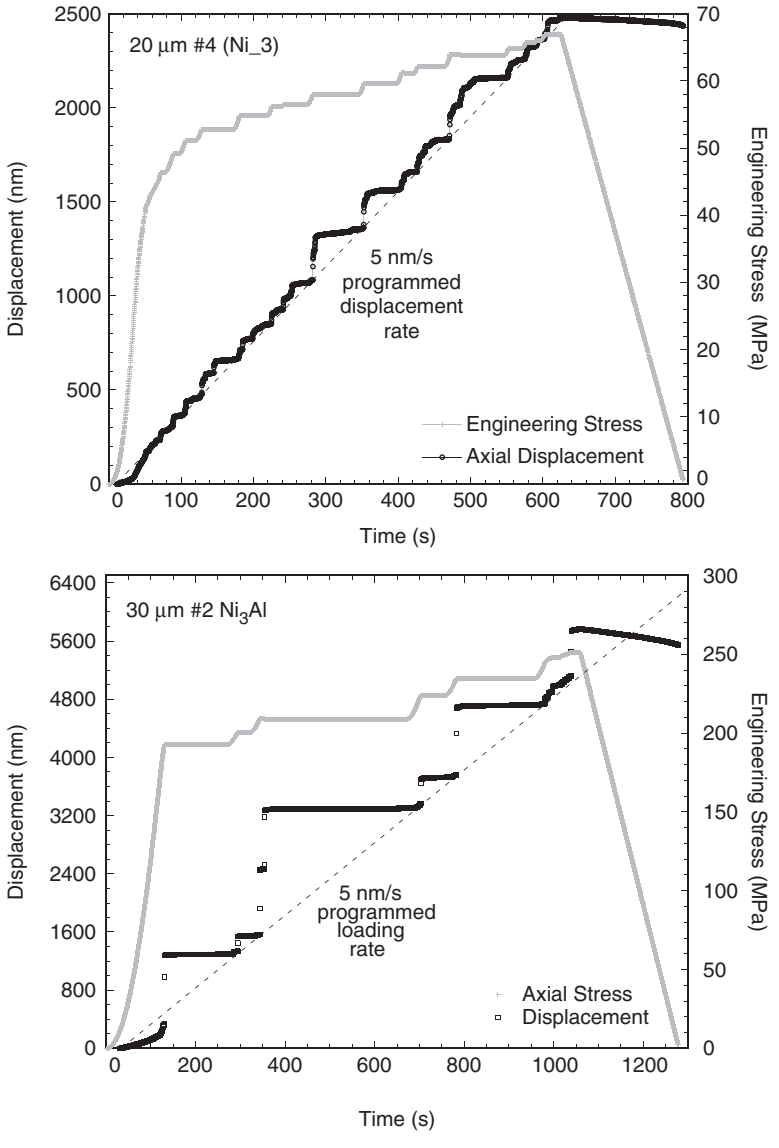

Figure 14. Compressive deformation of microsamples of pure Ni (top) and Ni_3Al (bottom); shown are stress vs. time and displacement vs. time curves as recorded in microtesting experiments (for details see text). Courtesy of D. Dimiduk.

up to comparatively large strains ($\gamma > 15\%$), leading to an extended Stage-I behaviour. At the same time, the deformation characteristics differ dramatically from those of bulk samples:

- Intermittency of plastic deformation becomes evident as plastic flow proceeds in irregular bursts separated by quasi-elastic loading intervals. During the deformation bursts, the plastic strain rate increases from near zero to very large values.

- As the stress is kept constant during each deformation burst, the stress–strain curves assume a shape reminiscent of a random 'devil's staircase' with an irregular sequence of steps of widely varying magnitude. We note that a similar step-wise increase of deformation with increasing stress may be observed in bulk samples on a local level, e.g. by monitoring the growth of slip bands [49, 60].
- The flow stress of small samples is larger than that of bulk specimens and increases as the specimen dimensions decrease. This size effect cannot be attributed to the presence of strain gradients and 'geometrically necessary' dislocations, which have become a commonplace explanation for size effects in plasticity (for an overview, see, e.g. [61]): Owing to the single-slip simple-shear geometry, no geometrically necessary dislocations accumulate in the deformation experiments under consideration. One has therefore to look for statistical explanations of the observed size effect.
- The burst-like character of deformation becomes more evident as the specimen dimensions decrease. At the same time, the stochastic nature of the flow process leads to increasing variations between deformation curves of different specimens, even if these have been machined out of the same single crystal and therefore share a common processing history.

The 'devil's staircase' nature of the stress–strain curves obtained from micron-sized samples is confirmed by statistical analysis. This reveals a scale-free distribution of step sizes (strain increments $\Delta\gamma$) with an exponent $\kappa_\gamma \approx 1.5$–$1.6$ [59]. The scaling regime is limited to about two orders of magnitude in step size, since smaller events are obliterated by the mechanical noise of the experimental setup, but above the noise threshold the power-law scaling is very convincing. Since plastic deformation is almost completely dissipative, the strain increment during a strain burst can be directly translated into the dissipated energy by multiplying it with the stress, $\Delta E = \tau \Delta\gamma V_s$ where V_s is the specimen volume. Neglecting the (small) stress increase due to hardening, we may therefore compare the exponent of the strain increment distribution observed by Dimiduk *et al.* and the energy exponent observed in AE recordings from deforming ice and hcp metals. This works out very well, as both exponents are between 1.5 and 1.6, indicating that both distributions may be governed by the same underlying physical processes.

3. Theoretical approaches

Different theoretical approaches have been used for investigating collective phenomena in plastic flow on microscopic and mesoscopic scales. These approaches differ in the way the deformation state is represented; however, as we shall see, the main results obtained from different approaches fit themselves into a consistent picture of plastic yielding as a non-equilibrium phase transition. In the following we shall discuss (i) models which describe plastic flow in terms of the motion of discrete lattice dislocations (dislocation dynamics); (ii) phenomenological models which describe plastic deformation in terms of the evolution of shear strain on crystallographic slip systems, and account for the influence of the underlying dislocation dynamics in terms of fluctuations in the local stress–strain relationship

(stochastic continuum models); (iii) phase-field models which take an intermediate position as they describe plasticity in terms of shear strain on crystallographic slip systems, but resolve the strain on a scale where individual dislocations can be identified as localized gradients of the strain field. Each of these models can be used to describe heterogeneity and avalanche phenomena in plastic flow, and the available results appear to be mutually consistent.

3.1. *Dislocation dynamics*

The most straightforward approach towards modelling plastic flow in crystalline solids on microscopic and mesoscopic scales is to investigate the stress-driven motion of interacting lattice dislocations. Individual dislocations or linear dislocation arrays interacting with randomly distributed obstacles may be treated within the general framework of elastic manifold depinning (see the introduction). In particular, it has been shown by Moretti and co-workers [27] that planar arrays of dislocations of the same sign (pile-ups or small-angle grain boundaries) exhibit long-range elasticity, with an elastic kernel Γ_P which in Fourier space scales in proportion with the modulus of the wavevector, $\Gamma_P \propto |\mathbf{k}|$ for $|\mathbf{k}| \to 0$. This implies that the motion of such arrays, depending on whether one is considering rigid or flexible dislocations, according to the terminology introduced in section 1.2 is in the class $a = d = 1$, or $a = 1$, $d = 2$. Simulations of the motion of a one-dimensional array of rigid dislocations through a pinning field reported by Moretti *et al.* indeed show exponents similar to those given for the $a = d = 1$ case in table 1. Interestingly, this seems to be true irrespective of whether the dislocations are arranged in an array perpendicular to their direction of motion (a grain boundary), or form a procession on the same slip plane (a pile-up) – even though in the latter case long-range correlations are present in the disorder as the dislocations move one after another through the same pinning field. For the physically realistic case of a planar array of flexible dislocations ($a = 1$, $d = 2$) one expects mean-field behaviour. Observations of the dynamics of such arrays via slip-line kinematography are consistent with this expectation (section 2.2.2).

For the dynamics of more general dislocation systems consisting of dislocations of different signs and/or moving on different slip systems, the depinning framework cannot be directly applied. One therefore has to rely on numerical simulations (section 3.1) for investigating the dynamic evolution of such systems under externally applied loads.

3.1.1. Simulation methods. Two-dimensional (2D) dislocation dynamics idealizes the dislocation system as a system of straight parallel lines. The simulations therefore essentially correspond to molecular dynamics simulations of particles moving in a plane. Three-dimensional (3D) dislocation dynamics, on the other hand, simulates the evolution of a system of flexible and reactive lines in three spatial dimensions. Both approaches have to cope with the fact that the dislocations are endowed with long-range ($1/r$) stress fields which cannot easily be truncated, and that the simulations therefore tend to be computationally expensive.

2D dislocation dynamics Two-dimensional dislocation dynamics is conceptually simple: Dislocations are envisaged as charged point particles in a plane.

Their motion is driven by the stress applied from outside to the deforming body, and they interact through long-range stress fields. If dislocation climb is neglected, the motion of these 'dislocation particles' is confined to the lines of intersection between the slip planes of the respective crystallographic slip systems and the simulation plane.

In most dislocation dynamics simulations, dislocation motion is assumed to occur in an over-damped manner. If dislocation glide is governed by electron and phonon drag forces, this leads to a linear relationship between the Peach–Koehler force $\mathbf{F}_{\mathrm{PK}}$ in the glide plane, and the dislocation glide velocity. The glide component of the Peach–Koehler force can be written as [cf. equation (8)]

$$\mathbf{F}_{\mathrm{PK}}(\mathbf{r}) = \mathbf{e}_g sb\tau(\mathbf{r}). \tag{30}$$

Here $\mathbf{e}_g$ is a unit vector pointing in the dislocation glide direction, the product sb of the sign $s = \mathbf{e}_g[\mathbf{t} \times \mathbf{n}]$ of the dislocation and the modulus b of its Burgers vector can be interpreted as the 'charge' of the 2D point particle representing the dislocation, and $\tau(\mathbf{r})$ is the local resolved shear stress in the dislocation slip system. Assuming a linear force–velocity relationship and considering dislocations of a single slip system only, one gets the system of equations

$$\mu\partial_t x_i = s_i\left[\tau + \sum_{k\neq i} s_k \tau_{\mathrm{D}}(\mathbf{r}_i - \mathbf{r}_k)\right], \tag{31}$$

where μ is the dislocation drag coefficient, the slip direction has been chosen to be the x direction, τ is the externally applied shear stress, and $\tau_{\mathrm{D}}(\mathbf{r})$ is the stress field of an individual dislocation. For an edge dislocation ($\mathbf{b} = b\mathbf{e}_x$) one has

$$\tau(\mathbf{r}) = \frac{Gb}{2\pi(1-\nu)}\frac{x\left(x^2 - y^2\right)}{\left(\mathbf{r}^2\right)^2}. \tag{32}$$

where ν is the Poisson number of the material. The local shear strain rate created by the dislocation system is

$$\dot{\gamma}(\mathbf{r}) = b\sum_k s_k \partial_t x_k \delta(\mathbf{r} - \mathbf{r}_k). \tag{33}$$

Simulations assuming a linear relationship between stress and dislocation velocity are very common both for 2D and 3D dislocation systems. However, it is important to note that experimental results on dislocation velocities show a much more complicated picture. As discussed in detail in the overview by Nadgorny [62], the dislocation velocity increases linearly with stress only in the high-stress regime, whereas at low stresses a strongly nonlinear (exponential) stress dependence is observed. For the dynamics of dislocation systems this is important, since at not too high applied stresses the motion of dislocations is strongly intermittent: The dislocations spend most of the time in low-stress configurations, which therefore control the mean velocity, and experience high stresses only during intermittent jumps between such configurations. The popularity of linear stress–velocity relationships has much to do with the fact that strongly nonlinear relationships increase the numerical stiffness of the simulations and may easily render their computational cost prohibitive. However, an easy and computationally efficient expedient for mimicking the effect of a strongly linear stress–velocity relationship is to use extremal dynamics

or automaton models where the dislocation moves (on the time scale considered) instantaneously to the next stable position whenever the stress exceeds a given threshold, and remains stationary otherwise. Results from such simulations will be discussed in the following, and compared to those obtained from simulations which assume linear stress–velocity laws.

Another important issue in 2D dislocation dynamics concerns the problem of dislocation multiplication. In deforming crystals, the total dislocation density (line length per unit volume) usually increases with increasing deformation, since the expansion of curved dislocation loops goes along with an increase in line length. Such 'dislocation multiplication' is important for two reasons: (i) In crystals with very low initial dislocation density, the proliferation of dislocations at the onset of deformation may lead to a transient softening. (ii) At larger dislocation densities, on the other hand, increasing the dislocation density increases the amplitude of the fluctuating internal-stress field in the deforming crystal and the strength of configurations in which dislocations mutually trap each other. The flow stress then increases according to the Taylor relationship, equation (34): the system exhibits strain hardening. Since loop expansion cannot occur in a system of straight lines, there is no straightforward method to account for dislocation multiplication in 2D dislocation dynamics. Researchers have tried to solve the problem by defining different kinds of phenomenological rules for introducing new dislocations into the system. However, as dislocations carry long-range stress fields, the creation of a new dislocation may discontinuously change the stress everywhere in the system, and thereby introduce all kinds of artefacts into the dynamics. To remedy this problem, several things can be done: (i) Dislocations should be introduced in pairs of opposite sign, since dislocation multiplication must conserve the total Burgers vector of the dislocation system. (ii) By placing the dislocations of such a pair close to each other, the stress discontinuity can be reduced. (If they are placed too close, however, because of their strong mutual attraction they will never become separated, and therefore contribute little to the dynamics.) (iii) By using different phenomenological rules, and comparing the outcomes, one may try to ensure that the results of a simulation do not depend crucially on the details of the dislocation multiplication rule.

A similar but less serious problem occurs if dislocations of opposite sign are allowed to instantaneously annihilate if their spacing falls below a certain cut-off distance. Computationally this is a ready expedient for reducing the computational stiffness of the simulations, since one avoids integrating the dynamics of configurations with large interaction forces. It is also physically less problematic than introducing dislocation multiplication since: (i) the total Burgers vector is conserved by definition in this process; (ii) the stress discontinuity due to the annihilation is small since the dislocations are close anyway; and (iii) the process is physically motivated, since straight edge dislocations of opposite sign have been observed experimentally to annihilate below distances of about $4b$ [63].

Another issue concerns initial and boundary conditions. In most simulations discussed in the following, periodic boundary conditions were imposed to mimic bulk behaviour. Initial conditions may be prescribed by distributing dislocations or dislocation sources according to some given statistical rule. In doing so it is important to note that a completely uncorrelated, statistically random initial

distribution of dislocations is unphysical since it implies an elastic energy density which diverges logarithmically with the system size [64]. One way to circumvent this problem is to use an initially random distribution but then, before studying the plastic flow dynamics, carry out a relaxation step at zero applied stress until the elastic energy of the system has stabilized. The relaxation of an initially random dislocation system is in itself an interesting, if somewhat academic, topic as it follows a slow dynamics governed by non-trivial power laws [65]. More interesting in view of the explanation of experimental observations is the subsequent evolution of the plastic deformation rate under constant applied stress, both in view of the creep behaviour and in view of the observation of intermittent avalanche-like dynamics (sections 3.1.2 and 3.1.3).

In most 2D dislocation dynamics simulations discussed in the following sections, the number of dislocations in a simulation has either been conserved, or a steady state with low rates of multiplication and annihilation (i.e. an almost conserved dislocation number) was reached and the influence of different rules for dislocation multiplication has been tested. One may therefore expect that the results of these simulations represent generic features of the dynamics of interacting dislocations and are not too heavily influenced by artefacts of the simulation technique.

3D dislocation dynamics Three-dimensional dislocation dynamics simulations is a science of its own. For a detailed discussion of such simulations, the reader is referred so some topical reviews [66, 67]. Problems similar to 2D are the long-range interactions between dislocation segments which cannot be truncated, and which in 3D make these simulations computationally very expensive. New problems arise from the necessity to describe a system of flexible lines with non-conserved line length, the need to maintain the connectivity of these lines, and the fact that two intersecting dislocations of different slip systems may react to create segments of a third slip system. For the scope of the present review, 3D dislocation dynamics simulations are of limited interest since the computational cost associated with such simulations has until now precluded their application to systems that are sufficiently large to detect long-range correlations and scale-free behaviour. Even though large systems have been studied in 'one-off' simulations, a proper statistical analysis of scale-free fluctuation phenomena in plastic deformation which involves the simulation of a large ensemble of systems has not yet been attempted. It may be expected that this situation will change in the near future, as the problem lends itself to 'trivial parallelization' on multiple computers, and standard computers may soon become powerful enough to run 3D dislocation dynamics simulations of appreciable size within acceptable time limits. At the same time, experimental observations can now be made on scales that are directly accessible to 3D simulation (see section 2.3 on micron-sized samples), allowing for a direct experimental validation of simulation results.

Scaling relations for dislocation systems Before discussing simulation results, it is useful to recall some general scaling relations which apply if the motion of dislocations is mainly controlled by their mutual interactions, rather than by lattice effects (Peierls stress) or by interactions with atomic defects or with precipitates. The stress field created by a dislocation in 2D scales like $1/|\mathbf{r}|$, and that created by a dislocation segment of length $\mathrm{d}s$ in 3D like $\mathrm{d}s/|\mathbf{r}|^2$. We now consider a dislocation arrangement

which is in (metastable) equilibrium at some external stress τ and decrease all distances by a factor λ. Since the dislocation density ρ is for a 2D dislocation system defined as the areal density of intersection points with a plane normal to the dislocation lines, and for a 3D dislocation system as the line length per unit volume, this operation in either case increases the dislocation density by a factor λ^2. Evidently, the new dislocation arrangement is in equilibrium at the stress $\lambda\tau$.

More generally speaking, if a dislocation arrangement of density ρ is in equilibrium at the stress τ, then an otherwise statistically equivalent arrangement of density ρ' is in equilibrium at the stress $\tau(\rho'/\rho)^{1/2}$. The same argument applies to loss of (meta)stability at some critical stress (yield stress) τ_c: the yield stress of a dislocation arrangement scales in proportion with the square root of dislocation density, as expressed by Taylor's relation

$$\tau_c = \alpha G b \sqrt{\rho}. \tag{34}$$

The scalar pre-factor α depends on the nature of the 'yielding transition'. For a single dislocation interacting with the stress fields of dislocations with density ρ threading its glide plane, yielding corresponds to the depinning transition of a weakly pinned elastic line [17]; if the dislocation can react with the threading 'forest dislocations', these are much stronger obstacles, and yielding may correspond to invasion percolation [68]; if we have a 2D system of straight interacting dislocation lines, the onset of plastic flow has been discussed in analogy with a jamming transition [69] (see next section). In either of these cases, the critical stresses for depinning/percolation/unjamming fulfil the Taylor relationship.

Some other scaling relations are also straightforward. Assuming that dislocation creation and annihilation are not prominent, the shear strain can be understood as the product of dislocation density and mean glide path, $\gamma = \rho b L$. Consider now a rearrangement in the dislocation system which produces a strain increment $\Delta\gamma$ in a system of linear extension L_s and dislocation density ρ. Trivially, a similar rearrangement in a statistically equivalent system of size L_s/λ and density $\lambda^2\rho$ produces a strain increment $\lambda\Delta\gamma$, since the glide path decreases like $\rho^{-1/2}$. We consider now the case where L_s is large enough such that boundary and finite-size effects are not important, and omit the re-scaling of the system volume. In this case, for the slip event $\Delta\gamma$ in the system with density ρ there is still an equivalent event in the system with density $\lambda^2\rho$. Referring the strain increment to the entire system, this event now produces the total strain increment $\Delta\gamma/\lambda^{d-1}$ where $d \in \{2, 3\}$ is the system dimension. The same scaling property holds for parameters such as the average, the median, or the 'largest' and 'smallest' events in an arbitrary event size distribution.

These scaling relations (often referred to as 'laws of similitude' in the metallurgical literature [14]) may seem trivial, but they have important consequences. They allow to deduce the behaviour of dislocation systems of different densities from a single set of simulations by means of simple scaling transformations. We use this in the simulations reported in sections 3.1.3 and 3.2.2 where we give lengths, stresses and strains in the respective 'natural units' $\rho^{-1/2}$, $Gb\rho^{1/2}$, and $b\rho^{1/2}$. Finally we shall use them, together with our simulation results, to obtain estimates of the magnitude and observability of dislocation avalanches in macroscopic deformation experiments (section 4.1).

3.1.2. Relaxation and creep of two-dimensional dislocation systems. Miguel *et al.* [69, 70] studied the creep relaxation of 2D dislocation systems consisting of equal numbers of dislocations of a single slip system, assuming a linear stress–velocity law. Periodic boundary conditions were imposed for the stresses and dislocation motions, the dislocations were initially placed at random and the initial configuration was relaxed at zero internal stress. A constant shear stress was then applied and the evolution of the shear strain rate $\mathrm{d}\gamma/\mathrm{d}t \propto \sum_i s_i v_i$ was monitored.

While the creep dynamics in individual simulations is strongly intermittent and characterized by irregular bursts [70], after averaging over many individual simulations a coherent picture emerges: During a transient after application of the external shear stress, the creep behaviour is characterized by power-law relaxation of the strain rate, with a relaxation exponent close to 2/3 ($\dot{\gamma} \propto t^{2/3}$, see figure 15). Accordingly, the creep strain increases in time as $\gamma \propto t^{1/3}$. After the initial transient, the deformation behaviour bifurcates depending on the applied stress: Below a critical stress, the deformation rate relaxes exponentially towards zero (the system gets jammed) whereas above the critical stress, the deformation rate becomes asymptotically constant. Power-law relaxation regimes of appreciable length can be found over a wide range of stresses. These findings compare well with Andrade's old observation of a 'universal', i.e. material-independent 'primary' or transient creep regime [71, 72] during which the creep strain increases like $\gamma \propto t^{1/3}$, and which is followed by a 'secondary' regime during which the creep rate is roughly constant.

Above the critical stress the system reaches an asymptotically constant creep rate. This statement is, however, correct only in the sense of a statistical average over many systems. In an individual simulation, the strain rate undergoes large fluctuations, and it has been attempted to relate these fluctuations to the acoustic emission bursts observed in ice single crystals that we have discussed in section 2.1.

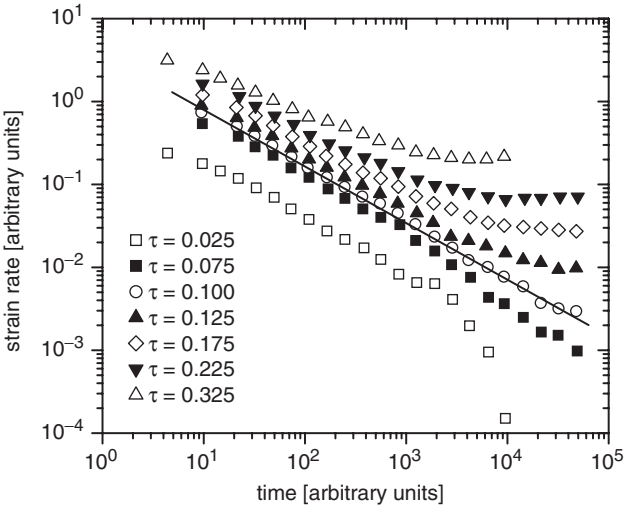

Figure 15. Strain rate relaxation of a 2D dislocation system for different applied stresses; stresses in units of $Gb\sqrt{\rho}$; the solid line is the best linear fit of the $\sigma = 0.1$ curve and yields $\mathrm{d}\gamma/\mathrm{d}t \sim t^{-0.69}$. After Miguel *et al.* [69].

Dislocation avalanches in creep deformation In several papers, Miguel *et al.* investigated the possibility of explaining experimentally observed AE signals in terms of the intermittent bursts of dislocation activity observed in their creep deformation simulations [5, 6]. In addition to the strain rate, they monitored the sum $V = \sum_i |v_i|$ of the absolute velocities of the dislocations. Since the friction force in the overdamped dynamics was assumed proportional to velocity, V is proportional to the energy dissipated per unit time by the dislocation system. One observes an intermittent and burstlike $V(t)$ signal on top of a continuous background. Provided that AE recordings provide a faithful representation of the dissipation characteristics of dislocation systems, it should be possible to relate the statistics of the simulated dissipation bursts to those of the experimentally observed AE signals.

To eliminate the continuous background, Miguel *et al.* used two methods: In one paper [5], a simple thresholding procedure was used to split the $V(t)$ signal into discrete bursts $\mathcal{B}$, and the energy dissipated during a burst was obtained as $E \propto \int_{\mathcal{B}} V(t)\mathrm{d}t$. The cumulative energy distribution obtained in this manner was observed to decay with an exponent $\kappa_E - 1 \approx 0.6$, which is in good agreement with the experimental observations discussed in section 2.1. In a second paper [6], the procedure was slightly different since only dislocations with velocities above the velocity corresponding to the externally applied stress were included in the evaluation of V. Since such 'fast' dislocations move in the direction imposed by the applied stress (this is not true for 'slow' dislocations, as will be discussed below), the value of V evaluated with the velocity threshold is in fact a proxy for their contribution to the overall strain rate. The acoustic energy was then defined as the square of V, which again lead to a power-law distribution with an exponent $\kappa_E \approx 1.8$ which is in acceptable agreement with experiment.

An interesting feature in the creep simulations of Miguel *et al.* is the presence of two physically distinct contributions to the strain and energy dissipation rates: (i) A major part of the dislocations at each moment is organized into slowly drifting multi-dislocation configurations (dipoles and multipoles). Dislocations of different signs form clusters which drift slowly into one or the other direction, depending on their net Burgers vectors and on the presence of stress gradients. Dislocations trapped in such clusters do not necessarily move in the direction imposed by the external stress. Since the clusters mostly have small net Burgers vectors, and their motion tends to be slow, they contribute little to the acoustic emission signal and even less to the strain rate. However, because of their large number such slowly moving dislocations still dissipate an appreciable amount of energy. (ii) The strain rate and acoustic emission signals are governed by small numbers of dislocations which break free from the slowly moving configurations and move rapidly under the action of external and internal stresses until they become trapped again. The rapid motion of one dislocation changes the stress everywhere in the system and may help other dislocations to break free. This mechanism is at the core of the observed avalanche dynamics. However, a quantitative analysis of the avalanche motion is complicated by the fact that the distinction between 'slow' and 'fast' dislocations requires the introduction of some artificial threshold. That such a threshold is somewhat arbitrary can be seen from the fact that the distribution $p(v)$ of the dislocation

velocities itself exhibits a power-law scaling regime, $p(v) \propto v^{-2.5}$ [6]. (Interestingly, this simulation result has received direct experimental confirmation in a recent investigation of Pertsinidis and Ling [73], who monitored the motion of edge dislocations during shear deformation of colloidal crystals.)

The problem of slowly moving dislocation configurations results partly from the assumption of a linear relationship between stress and dislocation velocity. Experimental investigations (for an overview, see the work of Nadgorny [62]) demonstrate that the velocity of dislocations is a linear function of stress only in the regime of high stresses, whereas at low stresses the velocity is governed by the interaction of dislocations with atomic defects, or with the Peierls potential of the crystal lattice, and therefore becomes a strongly nonlinear (exponential) function of the locally acting stress. This implies that multipole configurations, in which each dislocation experiences only a quite small stress, may be effectively immobile on the time scale of the experiment. Dislocation dynamics simulations with strongly nonlinear stress–velocity laws are computationally inconvenient, but the qualitative effect of a strong nonlinearity in the stress–velocity relationship can be easily assessed by using models with extremal dynamics (only the dislocation with the largest stress is allowed to move) or automaton models (dislocations move with unit velocity once the stress exceeds a threshold value). The results of such simulations indicate that the avalanche dynamics remains more or less unchanged, whereas the slowly moving configurations become 'frozen' and transform into effectively immobile trapping configurations [74].

3.1.3. Stepwise deformation curves and critical behaviour at yield. In a creep test the external stress is kept constant and the strain rate signal is recorded. During usual tension or compression tests, on the other hand, the applied stress is slowly increased from zero, and the stress–strain curve is recorded. There is a distinction between deformation-controlled tests where the stress is increased such as to maintain a given imposed deformation rate, and the stress is recorded as a function of time (strain), and stress-controlled tests where a constant stress rate is imposed and the strain is recorded. The distinction is, however, immaterial if one considers the deformation of a small volume embedded into a macroscopic crystal; in this case the local conditions always correspond to those in a stress-controlled test since local fluctuations of the deformation rate do not affect the stress applied from outside to the macroscopic deforming body.

The behaviour of dislocation systems during stress-controlled deformation testing was investigated by Zaiser *et al.* [74]. As in the simulations of Miguel and co-workers, deformation on a single slip system with equal numbers of positive and negative dislocations was considered and periodic boundary conditions were imposed. Also similar was the choice of initially random dislocation positions and subsequent relaxation of the dislocation system before an external stress was applied. However, an automaton technique was used for the dynamics: Dislocations were moved simultaneously on a discrete grid according to the sign of the locally acting stress, conditional on the requirement that the sign of the stress experienced by a given dislocation did not change during a move. The external stress was increased adiabatically slowly, i.e. an external stress increment was applied only after all

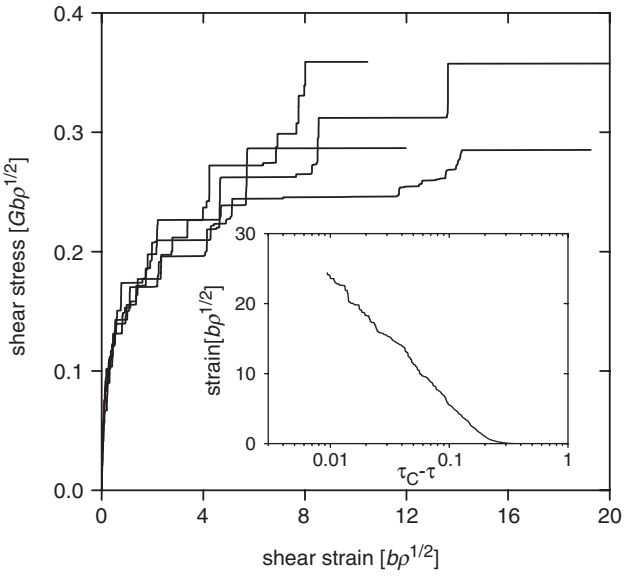

Figure 16. Stress–strain curves in simulated stress-controlled tests on systems of size 32×32 ρ (1024 dislocations); insert: average stress–strain behaviour obtained by averaging over 100 simulations.

dislocation activity had ceased. Alternatively, an extremal dynamics was used where only the dislocation with the largest stress was moved at a time, thus mimicking a strongly nonlinear stress–velocity relationship where all dislocations are practically at rest on the time scale of the fastest moving one. The dislocation number was conserved, i.e. neither dislocation multiplication nor annihilation were taken into account.

Stress–strain characteristics were determined by simultaneously recording the stress and the total strain $\gamma = (b/L_s^2)\sum_i s_i L_i$, where L_s^2 is the simulated area, s_i is the sign of the ith dislocation and $L_i = x_i - x_{i,0}$ is its (if necessary periodically continued) glide path. Simulations were terminated at a prescribed maximum strain. Results are shown in figure 16 where stress and strain are given in the respective 'natural units' for a dislocation system (cf. our discussion of scaling relations above). It is seen that the stress–strain curves assume a staircase-like shape similar to the experimental curves of micron-sized specimens discussed in section 2.3. Also in agreement with the experimental observations reported in that section is the fact that there is substantial scatter between different simulations. This scatter does not represent any differences in the material properties but simply reflects the outcome of different initial positions of the dislocations. Only after averaging over many simulations, can a smooth stress–strain characteristics be obtained, and it becomes evident that the strain diverges logarithmically as the stress approaches a critical value τ_c (yield stress, see insert of figure 16). The logarithmic divergence corresponds to a horizontal asymptote in the stress vs. strain graph, i.e. the model does not

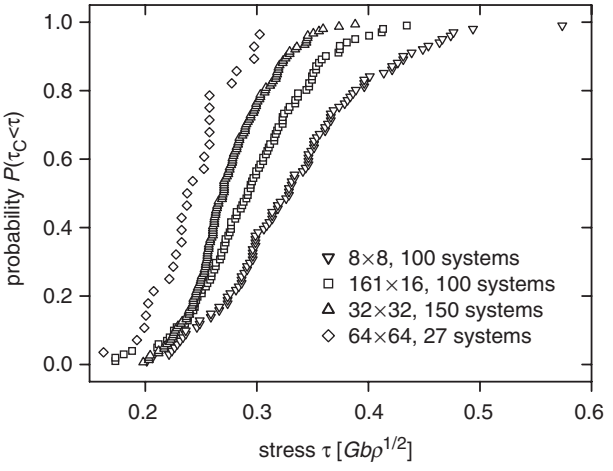

Figure 17. Distributions of yield stresses obtained for systems of different sizes (system size in units of $1/\sqrt{\rho}$).

display hardening. (This is to be expected, since no dislocation multiplication mechanism was introduced.)

The statistical distribution of critical stresses obtained from different simulations of statistically equivalent systems depends on system size. This is illustrated in figure 17 which shows probability distributions of yield stresses obtained from ensembles of systems of area $L_s^2 = 8 \times 8/\rho$ to $L_s^2 = 64 \times 64/\rho$ corresponding, for a typical dislocation density of $\rho = 10^{12}\,\mathrm{m}^{-1}$, to sizes of 8×8 to 64×64 ($\mu\mathrm{m}^2$). It is seen that the width of the distributions increases with decreasing system size, indicating an increasing scatter in the deformation behaviour. At the same time, the average yield stress increases for smaller systems. It is important to note that this size effect in the simulations is of a purely statistical nature and does not relate to surface effects or effects of dislocation sources, as periodic boundary conditions were used and a conserved number of dislocations was assumed. Both the increasing scatter and the increase in strength with decreasing system size match the observations in deformation of micron-sized specimens reported by Dimiduk *et al.* [57, 58], although the magnitude of the size effect is underestimated.

The behaviour in the individual simulations is characterized by large steps in the stress–strain curves (dislocation avalanches). The statistics of these avalanches has been investigated as a function of stress. Avalanches were characterized in terms of the total slip length increment $L_{\mathrm{av}} = \sum_i s_i \Delta L_i$ where ΔL_i is the difference between the positions of the ith dislocation before and after the avalanche. This makes it possible to directly compare simulations of systems of different area – the total strain increment $\Delta\gamma = bL_{\mathrm{av}}/L_s^2$, on the other hand, is inversely proportional to the simulated area L_s^2. Avalanche size distributions $p_\tau(L_{\mathrm{av}})$ were determined over narrow stress intervals centred around different stresses τ. Results are shown in figure 18 for $\Delta = (1 - \tau/\tau_c) = 0.2, \ldots, 0.8$.

One observes power-law distributions of dislocation avalanche sizes with a common exponent $\kappa \approx 1.4$. Whereas this exponent does not depend on stress,

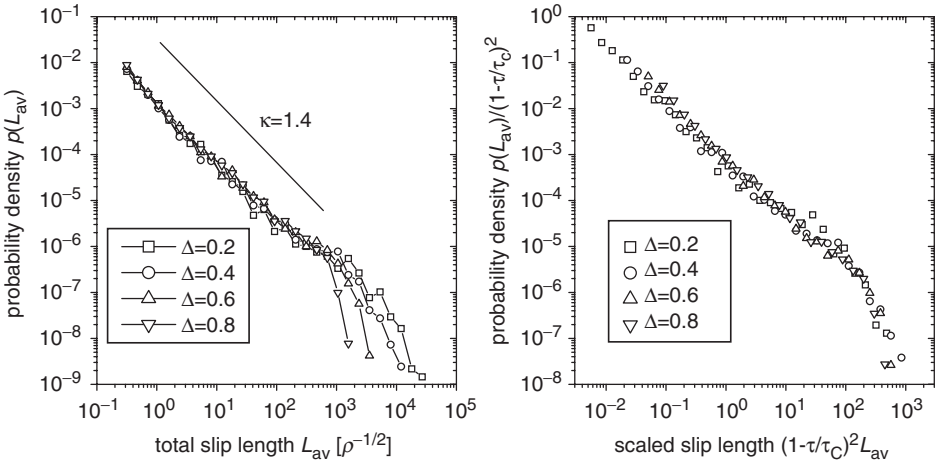

Figure 18. Distributions of dislocation avalanche sizes measured in terms of the total slip distance covered by dislocations during an avalanche; right: collapse of distributions obtained for different sized if size is re-scaled by $L_{av} \to L_{av}(1-\tau/\tau_c)^2$.

the maximum avalanche size increases like $(1-\tau/\tau_c)^{-1/\sigma}$ with $\sigma \approx 0.5$ as the stress approaches the yield stress. Accordingly, distributions pertaining to different stress levels obey the scaling form

$$p_\tau(L_{av}) = L_{av}^{-\kappa} f_L\left(\frac{L_{av}}{\Delta^{1/\sigma}}\right). \tag{35}$$

These distributions can therefore be collapsed by re-scaling $L_{av} \to L_{av}\Delta^{1/\sigma}$ (figure 18, right). It is also seen that power-law scaling is quite robust as scaling over more than three decades persists even at stresses that are just one fifth of the critical stress. This observation of robust scaling behaviour quite far from a critical point has also been made in other systems exhibiting avalanche dynamics [75].

In our model, the work $V_s\tau\Delta\gamma$ which is done by the external stress τ during an avalanche is completely dissipated. The proportionality between the energy dissipation and the strain increment (or equivalently the total slip length covered by dislocations during an avalanche) suggests a comparison between the avalanche exponent κ obtained from the present simulations and the energy exponent κ_E observed in the statistics of AE bursts. With $\kappa \approx 1.4$ and $\kappa_E = 1.5$–1.6 this comparison works out quite satisfactorily. The avalanche exponent $\kappa = 1.4$ also compares well with the exponent $\kappa_\gamma = 1.5$–1.6 of step size distributions from stress–strain curves of micron-sized samples [59].

At this point, we note that some caution is required when bursts from different parts of the stress–strain curve are added up. To illustrate the problem, we consider the *integral* distribution of avalanche sizes along the stress–strain curve as obtained from our simulations. This integral distribution is related to the stress-dependent distributions (which correspond to small stress intervals centred around

specific stress levels) via

$$p_{\mathrm{int}}(L_{\mathrm{av}}) \propto \int p_{\tau}(L_{\mathrm{av}})\mathrm{d}\tau \propto L_{\mathrm{av}}^{-(\kappa+\sigma)}. \tag{36}$$

Each of the distributions p_τ has the same exponent κ but a different cut-off. The integral distribution p_{int}, on the other hand, exhibits no cut-off but a modified avalanche exponent $\kappa + \sigma$ which by itself does not characterize the critical behaviour – rather, it combines two different exponents characterizing (i) the scaling regime of the avalanche size distribution and (ii) the scaling of its cut-off. This behaviour has been explicitly demonstrated in [74]. Of course, our consideration applies to a hypothetical non-hardening material and real materials with finite hardening coefficients may behave differently. Nevertheless it illustrates the dangers incurred when information is added up which pertains to different states of the system (i.e. to different separations from its critical point).

The behaviour of conserved two-dimensional dislocation systems with automaton or extremal dynamics under slow loading can be summarized as follows: (i) The strain diverges logarithmically as the stress approaches a critical value (yield stress). (ii) The response of the system to an increasing stress is characterized by an irregular sequence of strain bursts with power-law size distribution. (ii) This scale-free behaviour is manifest already at stresses well below the yield stress and persists up to a maximum burst size which diverges at yield. (iii) The exponents characterizing the critical behaviour (avalanche exponent $\kappa \approx 1.4$, divergence of the maximum burst size like $(\tau - \tau_{\mathrm{c}})^{-2}$) have approximately the values expected for mean-field depinning (see the introduction), even though the main ingredients of depinning models (dynamics of an elastic manifold, quenched disorder) are absent in the simulations.

To better understand the type of critical behaviour we are dealing with, it is useful to look at an apparently quite different class of models which operate on a scale where individual dislocations cannot be resolved and plastic deformation is described in terms of the evolution of a continuous plastic strain field.

3.2. *Models of microstrain evolution*

Dislocation dynamics directly traces the motion and collective dynamics of defects during plastic flow. Randomness, heterogeneity and stochastic behaviour in dislocation dynamics models stem from the probabilistic choice of initial conditions for the otherwise deterministic evolution of a discrete dislocation system. An alternative approach towards modelling collective phenomena in plastic deformation consists in the adaptation of continuum plasticity models to include microstructural heterogeneity and randomness in a phenomenological manner.

3.2.1. Constitutive equations. As discussed in the introduction, continuum mechanical constitutive equations connect the stress, plastic strain, and strain rate in a material. Such models operate on scales above the 'microscopic' scale where individual dislocations may be resolved. Accordingly, stress and strain must be considered as mesoscopic fields which are space dependent on a scale which is above the dislocation spacing, but small in comparison with the macroscopic

dimensions of the deforming body. Stresses associated with individual dislocations are not resolved, but enter the formulation implicitly since dislocation interactions determine the local yield stress of the material and its evolution with strain.

Deformation heterogeneities and internal stresses In the following we focus on the bulk behaviour of materials which are heterogeneous and random on microscopic and mesoscopic scales but homogeneous on the macroscopic scale. In this case the problem of evaluating the stress state of the material can be split into two parts: (i) Tractions applied from outside to the surface of the deforming body, or displacements prescribed on the surface of that body, create an 'external' stress $\mathbf{\Sigma}$ which we consider space-independent over the region of interest. (ii) Because of heterogeneities in the material properties, plastic deformation may in general proceed in a spatially heterogeneous manner on mesoscopic scales. Deformation heterogeneities give rise to eigenstresses $\mathbf{\Sigma}_{\text{int}}$. (A special case of such eigenstresses are actually the stresses associated with dislocations, where the heterogeneity corresponds to the boundary of a slipped area.) Provided that surface effects can be disregarded over the region of interest, the internal stress tensor can be written as a functional of the plastic strain field,

$$\mathbf{\Sigma}_{\text{int}}(\mathbf{r}) = -\mathbf{\Gamma}^0\left[\boldsymbol{\epsilon}^{\text{p}}(\mathbf{r}) - \langle\boldsymbol{\epsilon}^{\text{p}}\rangle\right] + \int \mathbf{\Gamma}^*(\mathbf{r}-\mathbf{r}')\boldsymbol{\epsilon}^{\text{p}}(\mathbf{r}')\mathrm{d}^3r', \tag{37}$$

where $\langle\boldsymbol{\epsilon}^{\text{p}}\rangle$ is the average plastic strain. Explicit expressions for the Green's functions $\mathbf{\Gamma}^0$ and $\mathbf{\Gamma}^*(\mathbf{r})$ have been given by Zaiser and Moretti for solids of arbitrary symmetry [76]. The special case of an incompressible isotropic material was considered by Picard *et al.* [77] where also the effect of boundaries was investigated.

In the following we consider the special case of an isotropic material deforming in plane strain on a single slip system. The slip planes are normal to the y axis, slip occurs in the x direction, and the strain field is assumed to be independent of z. This is equivalent to the deformation geometry investigated by 2D dislocation dynamics in the previous section. Plastic deformation is here completely characterized by the shear strain $\gamma = 2\epsilon^{\text{p}}_{xy} = 2\epsilon^{\text{p}}_{yx}$. The internal resolved shear stress in the considered slip system is given by [76, 78]

$$\begin{aligned}\tau_{\text{int}}(\mathbf{r}) = {} & \frac{G}{2\pi(1-\nu)}\int \gamma(\mathbf{r}')\left[\frac{1}{(\mathbf{r}-\mathbf{r}')^2} - \frac{8(x-x')^2(y-y')^2}{(\mathbf{r}-\mathbf{r}')^6}\right]\mathrm{d}^2\mathbf{r}' \\ & + \frac{G}{4(1-\nu)}[\langle\gamma\rangle - \gamma(\mathbf{r})],\end{aligned} \tag{38}$$

or, in Fourier space,

$$\tau_{\text{int}}(\mathbf{k}) = -\frac{G}{\pi(1-\nu)}\gamma(\mathbf{k})\frac{k_x^2k_y^2}{|\mathbf{k}|^4}. \tag{39}$$

Regarding these expressions, two points may be noted: (i) The elastic kernel is not positive definite in real space. (ii) Strain fluctuations with wavevectors parallel to the x or y directions do not give rise to internal stresses. The implications will be discussed below.

Constitutive equations: viscoplastic flow of a random material To relate the stress to the evolution of the strain field $\gamma(\mathbf{r})$, we adopt a linear viscoplastic constitutive relation of the type discussed in the introduction. The evolution of the local shear strain γ is given by [cf. equation (4)]

$$\mu\partial_t\gamma = \begin{cases} \big(|\tau+\tau_{\mathrm{int}}| - \tau_{\mathrm{y}}(\gamma,\nabla^2,\mathbf{r})\big)\mathrm{sign}(\tau+\tau_{\mathrm{int}}), & |\tau+\tau_{\mathrm{int}}| > \tau_{\mathrm{y}}(\gamma,\nabla,\mathbf{r}), \\ 0 & \text{else.} \end{cases} \tag{40}$$

Here τ is the externally applied resolved shear stress, τ_{int} is the internal shear stress due to deformation heterogeneities, and $\tau_{\mathrm{y}}(\gamma,\nabla,\mathbf{r})$ is the local yield stress. Randomness and heterogeneity in the material microstructure and microstructure evolution are taken into account in a phenomenological manner by allowing for a stochastic dependence of the yield stress on space and strain. Furthermore, internal length scales associated with the material microstructure can be taken into account by allowing the yield stress to depend on the second gradient of strain [12, 78].

In plastically deforming crystals, the local yield stress reflects the fine-scale dynamics of the interacting dislocations on scales below the spatial resolution of the mesoscopic model. For this case, Zaiser and co-workers [76, 78] proposed to relate τ_{y} to the fluctuating internal stress field created by the dislocations in the deforming crystal. This led to the following constitutive relation for the deformation resistance:

$$\tau_{\mathrm{y}}(\gamma,\nabla,\mathbf{r}) = -C\frac{\partial^2\gamma}{\partial x^2} + \delta\tau(\mathbf{r},\gamma). \tag{41}$$

The fluctuating stress $\delta\tau(\mathbf{r},\gamma)$ is associated with the 'microscopic' stress field created by individual dislocations. For a two-dimensional system of straight parallel dislocations of density ρ, it has the approximate correlation properties

$$\langle\delta\tau\rangle = 0, \quad \big\langle\delta\tau(\mathbf{r},\gamma)\delta\tau\big(\mathbf{r}+\mathbf{r}',\gamma+\gamma'\big)\big\rangle = \big\langle\delta\tau^2\big\rangle f_\tau\big(\mathbf{r}'/\xi_\tau,\gamma'/\gamma_{\mathrm{c}}\big), \tag{42}$$

where $\langle\delta\tau^2\rangle \approx G^2b^2\rho$, $\xi_\tau \approx 1/\sqrt{\rho}$ is the correlation length of the fluctuating stress field created by the dislocations, and f_τ is a non-dimensional correlation function with characteristic ranges ξ_τ and γ_{c} in its respective arguments. The 'correlation strain' $\gamma_{\mathrm{c}} \approx b\sqrt{\rho}$ was estimated as the strain accomplished when all dislocations move by the average dislocation spacing (for details see [76, 78] and references therein). Hardening may be introduced into the model by allowing the dislocation density and, hence, the amplitude $\langle\delta\tau^2\rangle$ of local stress fluctuations to increase with local strain. In particular, linear hardening corresponds to a quadratic increase of dislocation density with stress and strain. The term $C\gamma_{xx}$ in equation (41), in which $C \approx G/\rho$, stems from the short-range interactions between discrete dislocations moving on close slip planes (for derivation of this term, see Groma *et al.* [79]). This second-order gradient term scales in Fourier space like $\mathbf{k}^2\gamma(\mathbf{k})$ and is, hence, on large scales irrelevant in comparison with the long range elastic term, equation (39). However, the second-order gradient term has a decisive influence on the small-scale morphology of the deformation patterns, as it breaks the symmetry existing in the kernel in equation (38) between the x and y directions, and suppresses deformation heterogeneities in the direction of dislocation glide.

This turns out to be crucial for describing striated deformation patterns similar to the slip-line patterns observed in experiment.

The dynamics of the constitutive model specified by equations (38)–(42) exhibits a transition between a pinned and a moving phase, which corresponds to the depinning of an elastic manifold described by the equation

$$\mu \partial_t \gamma = \tau + \tau_{\text{int}} + C\gamma_{xx} + \delta\tau(\gamma, \mathbf{r}). \tag{43}$$

To see the analogy, we assume without loss of generality that the applied stress τ in equations (40) and (43) is positive and note that, apart from initial transients due to initial conditions, the local strain in both models increases monotonically under a positive stress. Hence, under a constant or increasing applied stress both equations yield the same asymptotic dynamics. In the hypothetical case of columnar disorder where the fluctuating stress $\delta\tau$ is a function of x and γ only, γ becomes independent on y, the internal stress τ_{int} vanishes, and elasticity is controlled by the second-order gradient term. In this case, the model becomes formally equivalent to the motion of a 1D manifold with local elasticity ($a = 2$) in a disordered medium. In the general case considered in the following, $\delta\tau$ depends on both x and y, and the elastic behaviour is on large scales governed by the long-range kernel of equation (38). Since $a = 0$ for this kernel, irrespective of space dimensionality one expects mean-field behaviour of the depinning transition.

We note that, even though part of the above discussion is specific to fluctuating internal stresses generated by crystal lattice dislocations, the general form of our equations is generic and can be applied to any material: The term $\delta\tau(\mathbf{r}, \gamma)$ – which in general may have non-zero average – statistically represents microstresses on the scale of the discrete elements whose dynamics governs plastic deformation, and the coupling term $C\gamma_{xx}$ (more generally $[\nabla \mathbf{C} \nabla]\gamma$) approximately describes short-range interactions on the scale of the size or spacing of these discrete elements. It is therefore not astonishing that the present constitutive formulation has many similarities with models of the plastic flow of amorphous solids and 'yield-stress liquids' as proposed by Barat *et al.* [80], Bulatov and Argon [81], and Picard *et al.* [82]. The model of Barat *et al.* generalizes ideally plastic behaviour to a material with random microstructure and microstructure evolution; the main difference with the present model – apart from the assumption of an extremal dynamics instead of linear viscoplasticity – is a different deformation geometry (plane vs. antiplane shear). The models of Bulatov and Argon, and Picard *et al.* on the other hand, use slightly different constitutive models for which yielding is associated with a strain softening instability.

3.2.2. Avalanche dynamics and surface morphology evolution.

Stress–strain curves and slip avalanches Stress–strain curves obtained from simulations of the continuum model detailed in the previous section are shown in figure 19. In this and in the following figures, length, stress, and strain are again measured in the respective 'natural units' $1/\sqrt{\rho}$, $Gb\sqrt{\rho}$, and $b\sqrt{\rho}$ for a dislocation system. In the case of simulations with hardening, the hardening coefficient $\mathrm{d}\tau/\mathrm{d}\gamma$ is accordingly measured in units of G, and the dislocation density ρ entering these scaling factors is understood as the initial density. All simulations are carried out with periodic

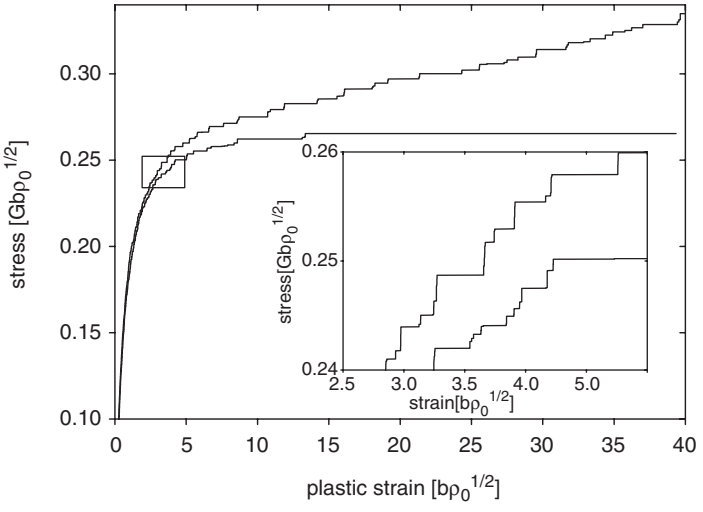

Figure 19. Stress–strain curves as obtained from simulation of a system of size 128×128 with zero hardening (lower curve) and with non-dimensional hardening coefficient of 3.5×10^{-3} (upper curve); insert: detail of the same stress–strain curves.

boundary conditions. It is seen from figure 19 that the simulated stress–strain graphs exhibit the same staircase-like characteristics as those observed in 2D dislocation dynamics simulations (figure 16). In the absence of hardening, the strain diverges at some critical stress τ_c where the stress–strain curve reaches a horizontal tangent. Averaging over many stress–strain curves shows that the susceptibility $\chi = \partial\gamma/\partial\tau$ of the plastic strain diverges according to $\chi \propto (\tau_c - \tau)^{-1}$, in the same manner as for the discrete dislocation model discussed in section 3.1.4 and in line with the expectation for mean-field depinning.

Close to the critical stress, the stress–strain curves have the structure of a 'devil's staircase' where the step sizes (sizes of slip avalanches) obey a scale-free distribution. Figure 20 shows distributions of step sizes $\Delta\gamma$ obtained over narrow stress intervals (width 0.01 in scaled variables) and at various distances from the critical stress. As one approaches the critical stress, the power-law scaling $p(\Delta\gamma) \propto \Delta\gamma^{-\kappa}$ with $\kappa \approx 1.4$ extends over a larger and larger range of scales, with the maximum size of the slip avalanches diverging like $(\tau_c - \tau)^{-2}$.

This behaviour is almost identical with that observed in the 2D dislocation dynamics simulations reported in section 3.1.4 (figure 18) and again the avalanche exponent κ may be favourably compared with the exponents deduced from deformation of micron-scale samples and from AE measurements. In fact, not only the shape of the distributions but also the absolute avalanche sizes are practically the same if one uses the relation $\Delta\gamma = bL_{tot}/L_s^2$ with $L_s = 256\rho^{-1/2}$ to convert between data in figures 20 and 18. This makes it plausible that both models, though conceptually different in their formulation, not only belong to the same universality class but describe the same physical reality.

Figure 21 shows avalanche size distributions determined for different hardening rates and stresses above the critical stress (macroscopic yield stress) of

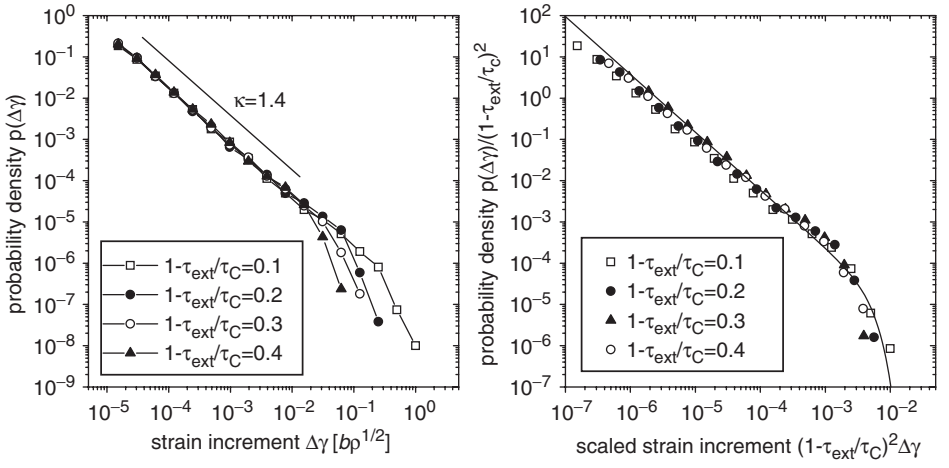

Figure 20. Probability distributions of slip avalanche sizes (probability density $p(\Delta\gamma)$ vs. strain increment $\Delta\gamma$) as obtained from an ensemble of systems of size 256×256; left: distributions corresponding to different stresses; right: universal distribution obtained by re-scaling $\Delta\gamma \rightarrow \Delta\gamma(1-\tau/\tau_c)^2$.

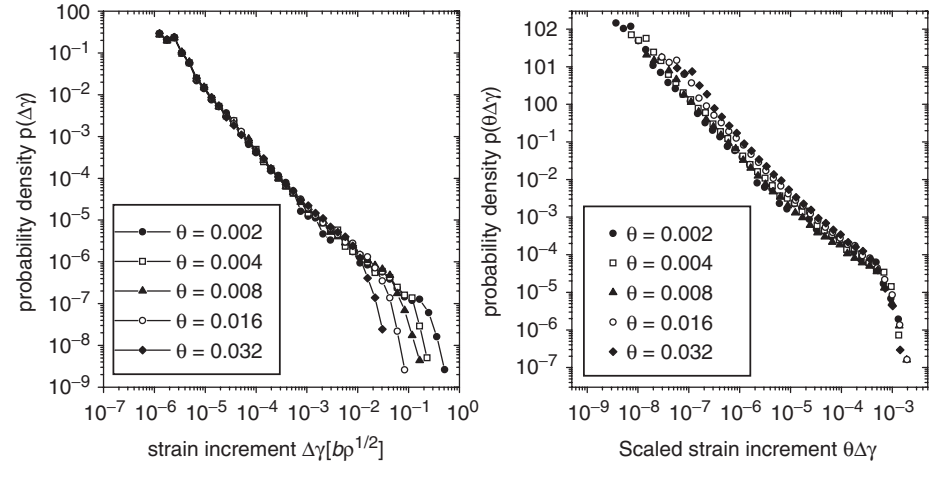

Figure 21. Probability distributions of slip avalanche sizes; left: distributions corresponding to different hardening rates; right: universal distribution obtained by re-scaling $\Delta\gamma \rightarrow \theta\Delta\gamma$.

a non-hardening system. It is obvious from figures 19 and 21 that hardening does not fundamentally change the stepwise morphology of the stress–strain curves or the power-law statistics, but eliminates the largest avalanches which, in a non-hardening system, occur at stresses close to the critical stress. In this sense, hardening suppresses the critical behaviour associated with the critical stress τ_c, but nevertheless leaves many of the scale-invariant properties of the dynamics unchanged.

The fact that the avalanche exponent $\kappa \approx 1.4$ is not changed by hardening compares well with the observations of Richeton *et al.* [45] on single crystals of hcp metals: During hardening stages I and II, the energy exponent $\kappa_E \approx 1.5$ was found to remain unchanged in spite of strongly differing hardening coefficients.

According to figure 21, in a strain-hardening system, the size of the largest slip avalanches is inversely proportional to the hardening coefficient. This can be easily understood from a scaling argument. With an avalanche exponent of $\kappa \approx 1.5$, the average strain $\Delta\gamma$ in an avalanche follows the relation $\langle\Delta\gamma\rangle \propto \Delta\gamma_{\max}^{1/2}$. Due to hardening, each avalanche raises the critical stress by a small amount $\Delta\tau_c \propto \theta\langle\Delta\gamma\rangle$, which implies that the external stress (which cannot instantaneously follow) lags behind the current critical stress by a similar amount. Finally, the maximum avalanche size follows the scaling relationship $\Delta\gamma_{\max} \propto (\tau_c - \tau)^{-2}$. Combining these relations, it follows directly that $\Delta\gamma_{\max} \propto 1/\theta$. We note that a very similar observation was made by Zapperi *et al.* regarding the influence of a demagnetizing factor on the motion of domain walls driven by an applied magnetic field through a disordered ferromagnet [26].

The hardening coefficients used in figure 21 ($\theta/G = 0.002, \ldots, 0.032$) tend to be above the range of hardening coefficients observed in single-slip deformation experiments on metal single crystals ($\theta/G = 10^{-4}, \ldots, 5 \times 10^{-3}$); the reason for this is simply that for smaller hardening coefficients the cut-off of the simulated avalanche size distributions becomes independent of θ, since it is then limited by the system size and not by the intrinsic dynamics of the system.

The stress–strain curves and avalanche statistics obtained from the time-continuous equation (40) are very similar to those obtained in [76, 78] from an automaton version of the same model, where the strain on the sites of a grid of unit mesh length was increased by a unit amount, and a new randomly chosen yield stress was assigned to that site, whenever the local stress exceeded the local yield stress. (The only perceptible difference between both models is that in the automaton model the critical stress is ca 20% higher for the same yield stress distribution.) However, the time-continuous model gives access to additional information in terms of the distribution of peak strain rates $\dot{\gamma}_{\max} =: A$ (evidently, a strain rate is difficult to define in an automaton model). Again, one observes a power law $p(A) \propto A^{-\kappa_A}$ with $\kappa_A \approx 2$, in good agreement with the peak amplitude distribution of AE bursts in ice (section 2.1). Irrespective of the hardening rate, no cut-off to the scale-free behaviour is apparent (figure 22).

Slip pattern and surface roughening Numerical simulation of the continuum model defined by equations (40)–(42) yields strongly anisotropic, striated strain patterns (figure 23) with strong correlations in the x direction (the direction of the slip plane) but weak correlations in the normal direction. This can be readily understood by looking at the elastic interactions in Fourier space: The Fourier transform of the elastic kernel is zero along the k_x and k_y directions, see equation (39). While fluctuations along the k_x direction are damped due to the second-order gradient term in equation (41), those along the y direction are not. The model is, hence, capable of representing at least qualitatively the slip anisotropy which in real crystals is a direct consequence of the glide motion of dislocations on slip planes.

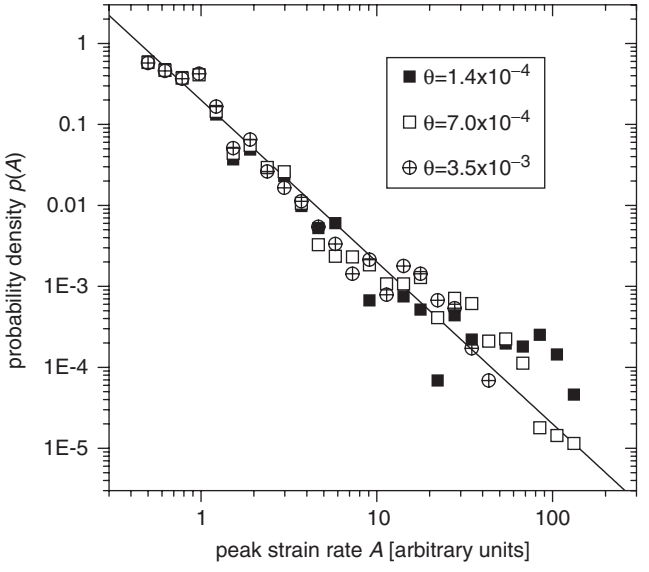

Figure 22. Probability distribution of peak strain amplitudes $A = \dot{\gamma}_{\max}$ obtained for different hardening rates. The distributions can be well approximated by a power law, $p(A) \propto A^{-2}$.

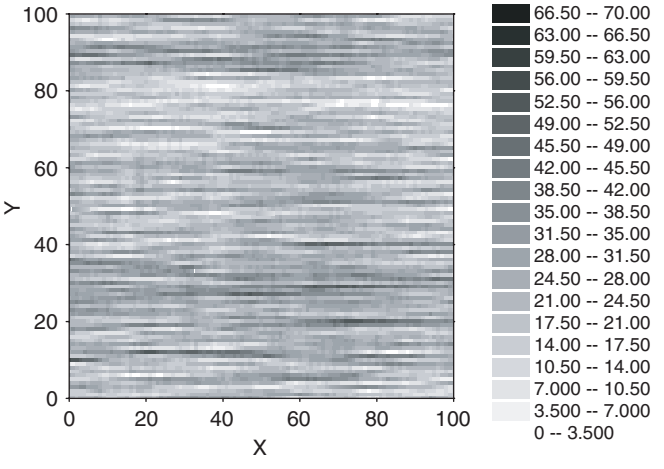

Figure 23. Strain pattern obtained after simulation of a system of size 256×256 to an average strain of $20b\sqrt{\rho}$ (slip direction from left to right); greyscale: local strain in units of $b\sqrt{\rho}$.

To compare with experimental findings (cf. section 2.2), one may integrate the strain profile along the y direction for some fixed $x = x_0$ to obtain a displacement profile along the corresponding plane normal to the slip direction:

$$y(x) = \int_0^x [\gamma(x) - \langle\gamma\rangle] \mathrm{d}x. \tag{44}$$

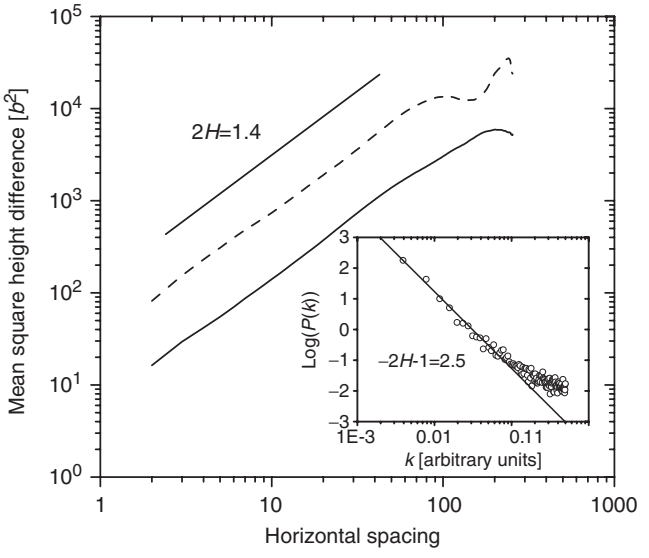

Figure 24. Mean square height difference vs. horizontal distance for surface profiles obtained from a system of size 512 × 512 after simulation to average strains of $6b\sqrt{\rho}$ and $20b\sqrt{\rho}$; each graph has been averaged over 10 simulated profiles; insert: Average power spectrum of the simulated surfaces for $\gamma = 20b\sqrt{\rho}$.

Assuming that surface-specific effects can be neglected (near a free surface, the elastic interactions are modified by the surface boundary conditions which are not taken into account in our model), the morphology of such simulated 'surfaces' may be compared with that of real ones.

Analysis in terms of self-affine roughness was performed by studying the height–height correlation function and the power spectrum of the simulated surfaces [76]. The results can be summarized as follows (see figure 24):

- The surfaces are self-affine up to a correlation length which is proportional to the size of the simulated system. They can be characterized by a strain-independent roughness exponent $\zeta \approx 0.7$.
- Increasing the total strain leads to growth of the profiles but does not change the roughness exponent or the correlation length (which is anyway determined by the system size). At large strains, the rms surface roughness on a given scale grows as the square root of strain.
- The numerical value of the roughness exponent compares well with the experimental observations, whereas the growth exponent of about 0.5 is slightly below the exponent of 0.8 observed during the single-slip deformation Stage I of KCl single crystals.

As discussed in section 2.2, self-affine surface roughness with a non-trivial roughness exponent $\zeta > 0.5$ points towards long-range correlations in the strain fluctuation pattern, with a strain fluctuation correlation function which decays like $r^{2\zeta-2}$. To elucidate the nature of such correlations in our simulations, it is useful

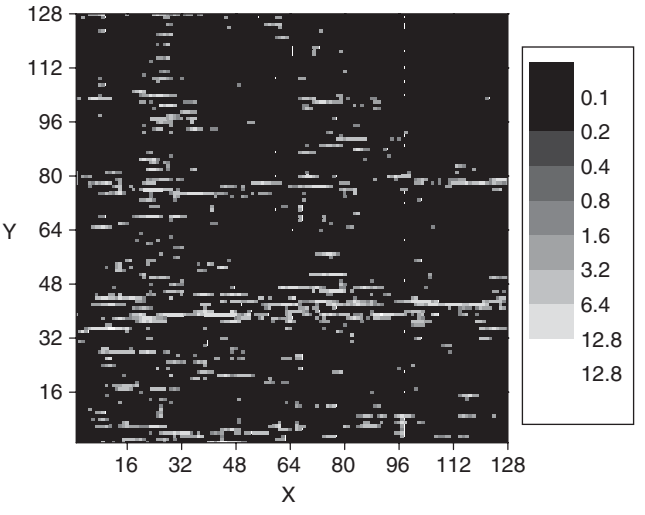

Figure 25. Strain distribution in a typical avalanche in a system of size 128 × 128 (greyscale values of local strain in units of $b\sqrt{\rho}$; the total strain increment in this avalanche averaged over the entire system is $\Delta\gamma = 0.5b\sqrt{\rho}$.

to investigate the spatial distribution of slip in an avalanche. A greyscale image of the slip distribution in a large avalanche is shown in figure 25. The slip distribution on small scales is characterized by striations parallel to the x axis. At the same time, long-range correlations are visibly evident both in the x and in the y directions.

These correlations can be quantified by calculating the correlation integral $C(R) = \int_{|\mathbf{r}-\mathbf{r}'|<R} \langle \Delta\gamma(\mathbf{r})\Delta\gamma(\mathbf{r}')\rangle \mathrm{d}^2(\mathbf{r}-\mathbf{r}')$. A power-law increase $C(R) \propto R^D$ of the correlation integral with non-integer D points towards a fractal pattern. From figure 26 one sees that linear scaling is approximately observed in large avalanches, with an apparent dimension of $D = 1.7$. Since the overall strain pattern is governed by the largest avalanches, this corresponds to a decay of the strain–strain correlation function like $r^{-0.3}$ which is consistent with a roughness exponent around 0.7.

3.3. *Phase-field models*

Phase-field models have an intermediate position between dislocation-based and continuum approaches towards plastic flow modelling. Similar to continuum approaches, the plastic deformation state is described by the evolution of strain variables. However, the strains are resolved on a 'microscopic' scale on which individual dislocations appear as localized gradients in the shear strain fields on the respective slip systems. The evolution of the local shear strains is derived from an elastic energy functional which includes not only long-range elasticity but also the Peierls energy of the crystal. The Peierls energy reflects the periodic structure of the atomic lattice and ensures that, in a stress-free crystal, the local shear strains take

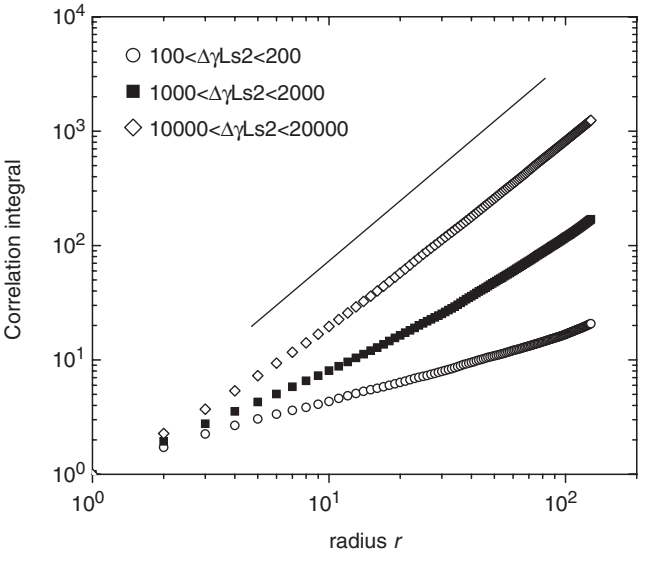

Figure 26. Correlation integrals of the strain distribution in avalanches of different size; the straight line has slope $D = 1.7$.

discrete values corresponding to displacements by multiples of the Burgers vectors of the respective slip systems.

Due to the description of the lattice strain on a quasi-atomic scale, the distinction between the stress (or the elastic strain) and the plastic strain becomes meaningless: Both quantities are described by the same variable, namely the relative displacement between two slipping lattice planes divided by their separation. We discuss in some detail the model proposed by Koslowski *et al.* [83, 84], who consider deformation on a single slip system and have applied their model to avalanche phenomena. This model envisages the two-dimensional distribution of slip on a single slip plane $z = 0$ in a three-dimensional continuum. (It is important to note that phase-field models are not restricted to single slip or planar systems. Phase-field modelling of multiple slip in three spatial dimensions, and the relation with 3D dislocation dynamics, has been discussed by Katchaturyan and co-workers [85]. The numerical simulation of such models is at present, however, computationally even more expensive than 3D dislocation dynamics simulations.)

Starting out from a continuous elastic–plastic shear strain field and a piecewise parabolic Peierls potential, Koslowski *et al.* [84] derive a formulation in which the plastic deformation field $\gamma(x, y)$ is represented as an integer-valued field with time-discrete dynamics. The deformation field at time $i+1$ is obtained from the field at time i by minimizing the incremental work function

$$W[\gamma(x,y,i+1)|\gamma(x,y,i)] = E[\gamma(x,y,i+1)] - E[\gamma(x,y,i)] + \int f(x,y)|\gamma(x,y,i+1) - \gamma(x,y,i)|\mathrm{d}x\mathrm{d}y \qquad (45)$$

where $E[\gamma(x, y, i+1)]$ is the elastic energy functional which in the presence of an external stress field $\tau(\mathbf{r})$ is given by

$$E[\gamma] = \frac{Gb^2}{4} \int \left\{ \frac{K}{1 + Kd_p/2} |\gamma(\mathbf{k})|^2 + \frac{\tau(\mathbf{k}) b \gamma(\mathbf{k})}{1 + Kd_p/2} \right\} \frac{\mathrm{d}^2 k}{(2\pi)^2}. \tag{46}$$

Here, $\tau(\mathbf{k})$ and $\gamma(\mathbf{k})$ are Fourier transforms of the fields $\tau(\mathbf{r})$ and $\gamma(\mathbf{r})$, d_p is the interplanar spacing, and

$$K = \frac{k_y^2}{\sqrt{k_x^2 + k_y^2}} + \frac{1}{1 - \nu} \frac{k_x^2}{\sqrt{k_x^2 + k_y^2}}. \tag{47}$$

The term $f(x, y)$ in equation (45) denotes the energy that is dissipated in changing the strain at the point (x, y) by a unit amount; it plays the role of a local obstacle strength which in [84] was assumed as a sum over randomly distributed point obstacles.

A detailed derivation of this model, starting from a continuous strain field and an energy functional with a piecewise parabolic Peierls potential, is given in [83]. Here we exclusively discuss the avalanche dynamics exhibited by the model as addressed in [84]. As an initial condition, Koslowski and co-workers in that paper assume a strain- and dislocation-free crystal under zero external stress. By increasing the external stress by small amounts and carrying out a sequence of minimization steps of the work functional given by equation (45), they demonstrate that the ensuing time-discrete dynamics exhibits a series of strain bursts with scale-invariant size distribution, with an approximately stress-independent exponent $\kappa_\gamma \approx 1.8$ for the distribution of strain increments.

While this is in itself an interesting finding and compares reasonably well with experimental observations, one objection may be raised against the procedure applied in these calculations. The discrete dynamics defined by equation (45) samples a sequence of energy minima but does not tell how the system gets from one minimum to another. That this may be a problem can be seen immediately by envisaging the moment when, under an increasing applied stress, the very first dislocation appears in the system. This happens as soon as the energy of a dislocation loop, trapped at obstacles somewhere in the system, falls below that of the dislocation-free crystal – a situation bound to be happen sooner or later since the loop, once created, reduces the elastic energy of the system by an amount proportional to the applied stress times the loop area. However, since the initial configuration is a dislocation-free crystal and only one slip plane is considered, dislocation sources do not exist and the loop has to be created *ex nihil*. It is easy to demonstrate that this process requires to overcome an energy barrier of prohibitive height, unless the applied stress is close to the theoretical shear strength of the ideal crystal. The model of Koslowski *et al.* does not 'see' this problem since it samples energy minima irrespective of the existence or non-existence of a path connecting them.

In spite of this flaw, the model has several interesting features. Spatial and temporal coarse-graining of the discrete-time dynamics given by equations (45)–(47) leads to

$$\frac{\partial \gamma(x, y)}{\partial t} = \frac{\delta E'(\gamma)}{\delta \gamma} + f(x, y, \gamma) \tag{48}$$

where the coarse-grained energy functional E' is given by

$$E[\gamma(x,y)] = \frac{Gb^2}{4}\int\left\{K|\gamma(\mathbf{k})|^2 + \tau(\mathbf{k})b\gamma(\mathbf{k})\right\}\frac{\mathrm{d}^2k}{(2\pi)^2}. \tag{49}$$

Equation (48) is the equation of motion of a two-dimensional manifold with long-range elasticity (the interaction kernel scales in proportion with the wavevector modulus k) moving through a random medium as characterized by the random dissipative force f. As discussed in the introduction, this model ($a = 1, d = 2$) is in the universality class of mean-field depinning. In fact, the motion of a two-dimensional pile-up of flexible dislocations as studied by Moretti *et al.* [27], which was found to be in the same universality class, can be treated within the framework of Koslowski *et al.* by using as initial condition for the strain field a constant strain gradient. The avalanche exponent observed by Koslowski and co-workers is somewhat above the value $\kappa = 1.5$ expected for mean-field depinning. The reason for this difference is not completely clear – it may be that Koslowski *et al.* include in their statistics events from the microplastic region well below the yield stress, which leads to an apparent increase of the avalanche exponent (cf. the discussion after equation (36)). It could also be that the difference is simply due to a technicality, since in [84] a linear instead of logarithmic binning procedure is used.

The model of Koslowski *et al.* provides a conceptual bridge between dislocation-based and strain-based models. As it stands, the model needs to introduce quenched disorder (the random dissipative force $f(x,y)$) in order to obtain metastable dislocation configurations. It remains a task for future work to generalize the model to more than one slip plane and investigate the possibility of self-pinning of the dislocation system in the absence of quenched disorder, which characterizes the discrete dislocation dynamics simulations discussed in section 3.1.

4. Discussion and conclusions

From the experimental and theoretical considerations discussed in the present review, a picture of crystal plasticity emerges which is at variance with the traditional paradigm of plasticity as a laminar flow process. The key elements of this picture may be summarized as follows:

(1) Plastically deforming crystals can under usual experimental conditions be envisaged as slowly driven non-equilibrium systems. The notion of 'slow' requires, however, some specification. This will be discussed in detail below.
(2) The dynamics of these systems is governed by the presence of a critical point marking a non-equilibrium phase transition ('yielding transition') of the dislocation system where, at a critical applied stress, the dislocations pass from a pinned/jammed to a moving phase.
(3) Critical behaviour manifests itself in terms of strongly intermittent dynamics with bursts of activity ('deformation avalanches') separated by quiescent intervals. The sizes of the avalanches obey scale-free distributions, characteristic of the intermittent 'crackling noise' associated also with other dynamical critical phenomena [46]. Both the spatial and the temporal distribution of the

avalanches are characterized by long-range correlations (spatial clustering, emergence of 'aftershocks'). There are indications that the spatial distribution of slip events follows fractal patterns [7, 48]. Scaling properties can also be observed in surface patterns where a self-affine surface morphology emerges during deformation.

(4) Observations of scale-free behaviour can be made on a wide class of metals and alloys. Details of crystal structure and alloy composition seem to be largely irrelevant – for instance, in the present review we find that the same model (section 3.2) can explain experimental observations made on ice, alkali halides, pure fcc metals, and superalloys. This robustness may indicate universality associated with the behaviour near the 'yielding transition'. Many of the theoretical and experimental results compiled in the present review indicate that this critical behaviour could simply be in the universality class of mean-field depinning.

It is obvious that this picture of plasticity owes a lot to the recent availability of convincing experimental data, in particular to the very comprehensive investigations of AE activity in ice carried out by Weiss and co-workers [6, 7, 36–41]. Given the fact that this as well as most of other experimental work reported in the present review uses techniques that have been available for decades, one may ask why the intriguing collective behaviour that can be observed during plastic deformation of crystals has escaped the attention of the physics and materials science communities until very recently.

4.1. *Why has it not been seen before?*

Some general observations A first and obvious response to this question leads us into the field of sociology (and psychology) of science. People tend to look for phenomena which they expect and understand, in other words, phenomena for which there is a conceptual and interpretative framework. A good scientist reports what he sees, but in the absence of such a framework, it is only too likely that some observations may not be followed up. In fact, jumps of the local strain which closely match the 'staircase-shaped' stress–strain curves of micron-scale samples (see section 3.1.3 and references) have been reported in the 1970s [60] and possibly even earlier. The experiments discussed in section 2.2.1, which demonstrated fractal slip patterns, date from the mid-1980s [48]. But only since the late 1980s has a conceptual framework been developed in which avalanche dynamics, crackling noise, and scale-free statistics are perceived as fairly general phenomena which are characteristic of a wide class of driven non-equilibrium systems. In the absence of such a framework, occasional observations of large fluctuations and scale-free behaviour reported in the materials literature remained unexplained and to some extent inconsequential.

In case of acoustic emission measurements, the situation is further complicated by the space and time scales involved. In the following it will be demonstrated that, depending on strain rate, hardening rate and dislocation density such measurements may yield either discrete or continuous AE signals, or a superposition of both, in spite of the fact that the underlying dynamics on microscopic and mesoscopic scales is the same in either case. Given the lack of explanation of 'crackling' signals, it is therefore quite natural that early research has usually focused on the continuous AE

as discussed in section 2.1.3. Even in cases where the crackling nature of the signal cannot be overlooked, as in the example shown in figure 5, no statistical analysis was performed since scale-free noise statistics were not considered a relevant or topical issue. In the opinion of the present author, however, continuous and discontinuous AE signals recorded during deformation of metals and alloys relate to the same fundamental physical processes which in ice single- and polycrystals give rise to an intermittent 'crackling' noise. We will show in the following why in metals discontinuous AE is often masked by an overlapping of signals emanating from different deformation bursts which is caused by the effect of a finite driving rate.

Deformation rate effects and the transition from discrete to continuous AE signals In plastic deformation of metals, one often observes transitions between discrete and continuous acoustic emission signals, as well as the simultaneous occurrence of both (spikes above a continuous background), cf. section 2.1.3 and figure 5. In this case, the continuous part of the signal may simply stem from the superposition of acoustic waves originating from independent bursts at different locations in the specimen. To assess the conditions under which this may occur, we consider a strain-rate controlled deformation test and define two critical strain rates: Above a critical strain rate $\dot{\gamma}_1$, the average time between two events falls below the mean event duration and a continuous background appears. At a second critical strain rate $\dot{\gamma}_2$, the magnitude of the continuous background becomes of the same order of magnitude as the characteristic amplitude $\Delta\gamma_{\max}$ of the largest bursts. Above this rate, crackling noise becomes altogether unobservable. If we make the simplifying assumptions that bursts occur uncorrelated in time, and the amplitudes of subsequent burst are statistically independent, these two critical strain rates can be estimated as

$$\dot{\gamma}_1 = \frac{\langle \Delta\gamma \rangle}{t_r}, \quad \dot{\gamma}_2 = \frac{\Delta\gamma_{\max}}{\langle \Delta\gamma \rangle}\dot{\gamma}_1 = \frac{\langle \Delta\gamma_{\max} \rangle}{t_r}. \tag{50}$$

Here t_r denotes the effective duration of a burst as recorded by the acoustic transducer. Because of reflections at the specimen surfaces, this duration is in general longer than the actual duration of the burst. A lower estimate for t_r is therefore given by the characteristic time for acoustic wave propagation, $t_r \geq c/L_s$ where L_s is the characteristic size of the specimen and c the longitudinal sound wave velocity. We finally note that, for stress controlled experiments, critical stress rates can be defined as $\dot{\tau}_{1/2} = \theta\dot{\gamma}_{1/2}$ where θ is the strain hardening coefficient or the inverse susceptibility, $\theta = (\partial\langle\gamma\rangle/\partial\tau)^{-1}$.

For a power-law burst size distribution with exponent $1 < \kappa < 2$ and upper and lower cut-off $\Delta\gamma_{\max}$ and $\Delta\gamma_{\min}$, the average strain increment in a burst is

$$\langle \Delta\gamma \rangle = \frac{2-\kappa}{\kappa-1}\ \Delta\gamma_{\max}^{2-\kappa}\Delta\gamma_{\min}^{\kappa-1}. \tag{51}$$

It is easy to see that, for a truly scale-free distribution where the upper cut-off diverges, the burstlike signal can always be observed. On the other hand, our investigation in section 3 has demonstrated that the distribution of event sizes is usually truncated at some large cut-off size. Such a cut-off in reality always exists. It may be due to intrinsic reasons (the stress is below the yield stress, or the material

exhibits strain hardening, cf. section 3.2). It may also result from the effects of finite grain size, or simply from the finite size of the deforming specimen.

Here we focus on the situation which is most relevant for assessing the observability of intermittent AE bursts in conventional deformation experiments, namely a single crystal of macroscopic dimensions which is deformed in strain rate control. (In polycrystals, the maximum event sizes are expected to be smaller and therefore bursts may be more difficult to observe.) We consider the upper critical strain rate $\dot{\gamma}_2$ which according to equation (50) depends on the maximum event size only. At lower strain rates, superposition of events may affect the statistical characteristics of the AE signal even though the 'crackling' nature of the signal is still manifest. For a discussion of these effects the reader is referred to the work by White and Dahmen [86].

We consider large events as a cascade of elementary ones, $\Delta\gamma_{\max} = N_{\max}\Delta\gamma_{\min}$. If plastic flow is controlled by dislocation interactions, the volume occupied by the smallest events is expected to be of the order of $\rho^{-3/2}$ and the strain produced within this volume to be of the order of $b\rho^{1/2}$ where ρ is the dislocation density (one dislocation segment moves by one 'wavelength' of the internal stress field, cf. the scaling relations discussed in section 3.1.1). The strain produced by an 'elementary event' within the macroscopic volume V_s of the deforming body is then given by $\Delta\gamma_{\min} = b/\rho V_s$. The number $N_{\max}$ does not depend on the dislocation density ρ but is, as discussed in section 3.2, inversely proportional to the strain hardening coefficient: $N_{\max} = CG/\theta$. From the simulation results of section 3.2 we obtain the estimate $C \approx 50$.

Throwing together all these relations, we can estimate the critical strain rate below which intermittent 'crackling' noise can be observed. We find that

$$\dot{\gamma}_2 \approx \frac{CbcG}{\theta V_s L_s \rho}. \tag{52}$$

We consider a Cu specimen with typical dimensions $L_s \approx V_s^{1/3} \approx 5$ mm, Burgers vector length of $b = 2.5\,\text{Å}$, and typical dislocation densities and hardening coefficients in hardening stages I and II. In Stage I, $\theta/G \approx 5 \times 10^{-4}$ and $\rho \approx 10^{12}\,\text{m}^{-2}$ which yields a value $\dot{\gamma}_2 \approx 2.5 \times 10^{-4}\,\text{s}^{-1}$ which is well within the usual range used in deformation tests. In Stage II, on the other hand, typical dislocation densities are one or two orders of magnitude larger and the hardening coefficient increases by up to a factor of 10, $\theta/G \approx 5 \times 10^{-3}$ and $\rho \approx 5 \times 10^{13}$ which leads to a critical strain rate $\dot{\gamma}_2 \approx 5 \times 10^{-7}$ which is well below the usual experimental range. These estimates compare well with observations of Imanaka *et al.* [42] who observed burstlike AE during the initial loading of a Cu single crystal of high purity and very low initial yield stress ($\tau < 1\,\text{MPa}$) which after deformation to a flow stress of about 3 MPa (corresponding to a tenfold increase in dislocation density) gave way to a continuous AE signal. The observation of crackling noise in hcp metals, where Stage II dislocation densities and hardening rates tend to be lower than in fcc metals, fits into the same picture, as does the fact that Weiss *et al.* made their observations on ice single crystals with extremely low initial dislocation densities ($\rho \sim 10^8\,\text{m}^{-2}$).

These estimates indicate that observability of burstlike AE induced by dislocation plasticity can under usual experimental conditions not be taken for granted even in fcc metals where dislocation mobilities are high. The situation may be different in

deformation by twinning, where the elementary events are much larger, and/or in the presence of plastic instabilities. However, our estimates also demonstrate that macroscopically continuous AE signals need not be at variance with an intermittent avalanche dynamics on mesoscopic and microscopic scales which, in the case of the simulation data of figure 21 on which our estimate is based, exhibits scale-free behaviour over five orders of magnitude in avalanche size.

4.2. *Open questions, doubts and prospects*

In this review we argue that scale-free fluctuation patterns in crystal plasticity represent critical behaviour associated with a non-equilibrium critical point ('yielding transition'). However, critical behaviour is by definition confined to an isolated point in parameter space: critical phenomena are not generic. Furthermore, a plastically deforming crystal is not actually in a steady state: Since plasticity leads to microstructural changes (dislocation multiplication, strain hardening), ongoing deformation requires an continuously increasing stress. Hence, in strain hardening materials (i.e. in most crystalline solids) the point of yielding, in the sense of sustained flow under constant stress, is actually never reached: If the yield stress marks a critical point, the system chases the ghost of that point as each stress increment leads to plastic activity which in turn, due to the ensuing microstructural changes, moves the point of yielding towards higher and higher stresses.

There are two ways to reconcile these observations with the fact that, as demonstrated in this review, scale-free fluctuations are a fairly general feature of crystal plastic flow:

(i) Several authors have adopted the notion of self-organized criticality (SOC). SOC in the context of plasticity means that there is some mechanism which ensures that the evolving dislocation system settles into a state where the applied stress corresponds precisely to the momentary yield stress. Indeed, the model discussed in section 3.2 of the present review is closely related to a model proposed by Bak and co-workers for describing the 'self-organized critical' dynamics of shearing processes at earthquake faults [87]: The SOC model of Bak *et al*. actually implements an automaton version of the continuum model in section 3.2, with a particular choice of the hardening coefficient. This observation, however, rather than advocating the concept of SOC for plasticity, indicates that the model of Bak *et al*. is actually not evolving towards a truly critical state (cf. the discussion of hardening in section 3.2). The fact that Bak *et al*. in [87] do not find any intrinsic limits to the scaling regimes of their avalanche size distributions has the simple reason that their system sizes are too small. As a consequence, they find scaling over two decades, whereas our results in section 3.2 even for large hardening coefficients indicate robust scaling over four decades before the intrinsic cut-off proportional to the hardening coefficient becomes manifest.

(ii) The concept we prefer is that of 'robust scaling': the dynamics of a system may exhibit scaling behaviour associated with a critical point even if the system is *not* very close to that point in parameter space. Our investigations have revealed several examples of such robust scaling – see, e.g. the avalanche size distribution in figure 18, where scaling behaviour over almost four decades is observed at stresses that are just 20% of the critical stress.

If plastically deforming crystals are not in a truly critical state, this has the important implication that, in sufficiently large samples, fluctuations will finally average out. In terms of the acoustic emission, we have demonstrated that small uncorrelated AE events from different parts of the crystal may superimpose to produce the continuous AE background commonly observed in AE experiments on metals and alloys. Similarly, in macroscopic deformation experiments the superposition of many small and uncorrelated strain increments obliterates the staircase-like structure of the stress–strain curves that is blatantly manifest from small samples. Another implication of a possible *absence* of true criticality is that spatial correlations in the plastic flow pattern may have a finite range, above which the traditional homogenization methods of continuum mechanics can be successfully applied. In fact, it may be wise to make the modest claims of 'nearly critical' or 'robust critical' behaviour, as opposed to SOC, in order to avoid the impression that the methods of continuum mechanics (including homogenization methods and the use of conventional constitutive equations in crystal plasticity) as used during the last 200 years were completely off the mark.

When it comes to predicting plasticity on the micron scale, as for instance in microelectromechanical systems, however, these caveats do not hold and conventional constitutive equations, which imply deterministic materials behaviour, may indeed be quite inadequate to account for plastic behaviour which on these scales is intrinsically controlled by fluctuation phenomena.

Several observations still remain vexatious:

(1) In the creep experiments on ice, changing the stress over a wide range leaves the energy distribution of AE bursts virtually unchanged, and no indication of a cut-off can be found over more than 6 decades in energy. Moreover, the same distribution seems to govern the AE burst energies in different creep regimes during which the *average* creep rates differ by orders of magnitude. No presently available model seems capable of reproducing or understanding this extremely robust behaviour. The 'SOC viewpoint' would of course be that, whatever the stress, the system is self-organizing towards its critical point. However, a physically motivated model which provides a mechanism for such self-organization in a dislocation system has yet to be formulated.

(2) The interpretation of AE experiments hitherto relies on extremely simplistic models assuming compact sources. The theoretical investigations, on the other hand, indicate that the acoustic source during a 'slip avalanche' may have a complicated structure: owing to the long range of elastic interactions, dislocations may move in a correlated manner in spite of being widely separated, and the effective source may be a fractal dust rather than a compact object. One may ask whether the simplistic assumptions underlying the current interpretation of AE measurements affect the results, in particular the avalanche exponents. To clarify this point, one might investigate how the predictions of an AE source model based on one of the models described in section 3 would differ from those based on a simple coherent or incoherent superposition of compact sources as assumed in the analysis of previous experiments.

(3) All presently available models are formulated for single crystals and simple deformation geometries, where the plastic strain and strain rate can effectively be treated as scalar fields and the stress as a scalar driving force. The same holds for many of the available experiments, which have been conducted on single crystals deforming in single-slip geometries. The behaviour of more general models which necessarily have to take into account the tensorial nature of stress and strain may be substantially different, as the dimensionality of the order parameter of the 'yielding transition' (i.e. the strain rate) is evidently an important issue for any kind of critical behaviour. There is experimental evidence for differences between single and multiple slip in the acoustic emission signals recorded during deformation of ice polycrystals, which differ substantially from those recorded during single crystal deformation: Not only does the size distribution of acoustic emission events in polycrystals exhibit a grain size dependent cut-off, but also the avalanche exponents are quite different from those for single crystals. There may be different reasons for these observations: (i) Grain boundaries may act as dislocation obstacles, and the blocking of slip at grain boundaries may cause strong kinematic hardening, as well as overstresses in adjacent grains. This is especially pronounced in ice where the activation of other than basal slip systems is difficult. (ii) In polycrystals (with the possible exception of ice), multiple slip systems operate simultaneously in most grains. To assess the respective influences of grain boundaries and multiple slip, both specific experiments (e.g. on single crystals deforming in symmetrical multiple slip) and corresponding theoretical models are needed.

(4) Many aspects of the avalanche statistics seem to be consistent with mean-field depinning, and the results obtained from simulations of discrete dislocation as well as of continuum models (section 3) point into the same direction. This is not unexpected owing to the long-range nature of the elastic interactions. However, the applicability of the depinning framework, and indeed the very existence of a unique depinning threshold (yield stress), is in no way guaranteed since the lack of positive definiteness of the interaction kernels prevents the application of Middleton's 'no passing' theorem for proving the existence of a unique threshold [88].

(5) An important question concerns the relations between the spatial and temporal structure of plastic flow. It is obvious that mean-field arguments by definition cannot tell us anything about the spatial structure of a process. The investigations discussed in section 3.2 indicate that the strongly anisotropic structure of the elastic kernels, which follows from continuum elasticity, may be crucial for the properties of strain patterns. Several questions remain unanswered: How can the observed spatio-temporal clustering of slip avalanches be explained? Can the existing models reproduce the fractal distribution of avalanche loci in a macroscopic sample as proposed in [7]? Is there a theoretical explanation of the observed surface roughening beyond the coincidence of experimental and simulation results?

A further issue which creates complications is the fact that the present models tend to over-simplify the properties and the evolution of the crystal defect

microstructure during deformation. The applicability of the depinning framework hinges on the presence of a statistically homogenous field of quenched disorder with short-range correlations. In the present context this translates into the assumption of a disordered and evolving, but at the same time statistically stationary dislocation microstructure. This assumption is acceptable in the sense that on the typical strain scale of individual slip avalanches the microstructure does not change a lot, and on the strain scale where it *does* change, the slip avalanches are truncated due to the ensuing hardening as discussed in section 3.2. Complications arise, however, from the following observations: Not only the dislocation density and the amplitude of the internal-stress fluctuations increase during deformation, but at the same time the characteristic 'wavelength' of the dislocation microstructure, and the correlation length of the stress fluctuations, decrease in proportion with the dislocation spacing. In the model of section 3.2, only the amplitude growth has been considered while the spatial 'shrinking' of the pinning field has been neglected. Another complication stems from the fact that, under certain deformation conditions, dislocations may arrange into fractal patterns, with a fractal dimension that increases during deformation [9, 10]. This implies that the pattern of local yield stresses may itself possess long-range correlations, and these correlations may not be stationary.

Many of the observations and models discussed in this review are not confined to crystal plasticity, but apply to any kind of shear flow. Hence, it is not unexpected that the models discussed in the present review bear close relations to models used in other contexts. A prominent example is the model of Bak and co-workers of earthquake dynamics [87] which is analogous to the continuum plasticity model of section 3.2. Another example is the amorphous materials plasticity model by Roux *et al*. [80] which considers a different deformation geometry (anti-plane instead of plane shear) but can be translated into crystal plasticity language in a straightforward manner: The model corresponds to the antiplane shear of a 2D crystal lattice with two symmetrical slip systems, while the other characteristics are essentially the same as in the model of section 3.2. It is hoped that future systematic investigations of these and related models will yield a unified picture of the irreversible deformation of both crystalline and amorphous solids, which allows to analyse and classify both the universal and the materials and geometry-specific features of plasticity.

Acknowledgments

M.Z. gratefully acknowledges numerous and stimulating discussions with S. Zapperi, J. Weiss, M.-C. Miguel, M. Alava, and E.C. Aifantis, as well as the collaboration of J. Schwerdtfeger, E. Nadgorny, P. Moretti, F. Madani, and A. Konstantinidis. Finally, the hospitality of CNR, Istituto di Sistemi Complessi, Rome, Italy, during the period in which this review was written is gratefully acknowledged.

References

[1] L.P. Kubin, Y. Estrin and E.C. Aifantis, Scripta Metall. Mater. **29** 1147 (1993).
[2] M. Zaiser and P. Hähner, Phys. Stat. Sol. (b) **199** 267 (1997).

[3] L.P. Kubin, C. Fressengeas and G. Ananthakrishna, in *Dislocations in Solids*, Vol. 11, edited by F.R.N. Nabarro and M.S. Duesbery (Amsterdam, North-Holland, 2002), pp. 101–192.
[4] M. Zaiser, Mater. Sci. Engng. A **309–310** 304 (2001).
[5] M.-C. Miguel, A. Vespignani, S. Zapperi, *et al*., Mater. Sci. Engng. A **309–310** 324 (2001).
[6] M.-C. Miguel, A. Vespignani, S. Zapperi, *et al*., Nature **410** 667 (2001).
[7] J. Weiss and D. Marsan, Science **299** 89 (2003).
[8] M. Zaiser, F. Madani, V. Koutsos and E.C. Aifantis, Phys. Rev. Lett. **93** 195507 (2004).
[9] P. Hahner, K. Bay and M. Zaiser, Phys. Rev. Lett. **81** 2470 (1998).
[10] M. Zaiser, K. Bay and P. Hähner, Acta Mater. **49** 2463 (1999).
[11] E.C. Aifantis, Int. J. Engng. Sci. **30** 1279 (1992).
[12] E.C. Aifantis, J. Eng. Mater. Tech. **121** 189 (1999).
[13] M. Zaiser and P. Hähner, Mater. Sci. Engng. A **238** 399 (1997).
[14] M. Zaiser and A. Seeger, in *Dislocations in Solids*, Vol. 11, edited by F.R.N. Nabarro and M.S. Duesbery (Amsterdam, North-Holland, 2002), pp. 1–100.
[15] J. Friedel, *Dislocations* (Pergamon Press, Oxford, 1967).
[16] B. Devincre and M. Condat, Acta Metall. Mater. **40** 2629 (1992).
[17] S. Zapperi and M. Zaiser, Mater. Sci. Engng. A **309–310** 348 (2001).
[18] H. Leschhorn, T. Nattermann, S. Stepanow and L.H. Tang, Ann. Physik **6** 1 (1997).
[19] D.S. Fisher, Phys. Rep. **301** 113 (1998).
[20] P. Chauve, T. Giamarchi and P. Le Doussal, Phys. Rev. B **62** 6241 (2000).
[21] P. Le Doussal, K.J. Wiese and P. Chauve, Phys. Rev. B **66** 174201 (2002).
[22] R. Labusch, Cryst. Lattice Defects **1** 1 (1969).
[23] R. Labusch, Acta Metall. **20** 917 (1972).
[24] A.I. Lar'kin, and Yu.N. Ovchinnikov, J. Low Temp. Phys. **34** 409 (1979).
[25] F. Family and T. Vicsek, J. Phys. A, **18**, L75 (1985).
[26] S. Zapperi, P. Cizeau, G. Durin and H.E. Stanley, Phys. Rev. B **58** 6353 (1998).
[27] P. Moretti, M.-C. Miguel, M. Zaiser and S. Zapperi, Phys. Rev. B **69** 214103 (2004).
[28] D. Cule and T. Hwa, Phys. Rev. B **57** 8235 (1998).
[29] S. Ramanathan and D.S. Fisher, Phys. Rev. B **58** 6026 (1998).
[30] U. Nowak and K.D. Usadel, Europhys. Lett. **44** 634 (1998).
[31] L. Roters, A. Hucht, S. Lübeck, U. Nowak and K.D. Usadel, Phys. Rev. E **60** 5202 (1999).
[32] M. Paczuski, S. Maslov and P. Bak, Phys. Rev. B **56** 414 (1996).
[33] D. Rouby, P. Fleischmann and C. Duvergier, Phil. Mag. A **47** 671 (1983).
[34] D. Rouby, P. Fleischmann and C. Duvergier, Phil. Mag. A **47** 689 (1983).
[35] V.D. Natsik and K.A. Chishko, Sov. Phys. Solid State **20** 1117 (1977).
[36] J. Weiss and J.-R. Grasso, Phys. Chem. B **101** 6113 (1997).
[37] J. Weiss, F. Lahaie and J.-R. Grasso, J. Geophys. Res. **105** 433 (2000).
[38] J. Weiss, J.-R. Grasso, M.-C. Miguel, *et al*., 2001, Mater. Sci. Engng. A, **309-310**, 360.
[39] J. Weiss and M.-C. Miguel, Mater. Sci. Engng. A **387–389** 292 (2004).
[40] T. Richeton, J. Weiss and F. Louchet, Acta Mater. **53** 4463 (2005).
[41] T. Richeton, J. Weiss and F. Louchet, Nature Mater. **4** 465 (2005).
[42] T. Imanaka, K. Sano and M. Shimizu, Crystal Lattice Defects **4** 57 (1973).
[43] N. Kiesewetter and P. Schiller, Phys. Stat. Sol. (a) **38** 569 (1976).
[44] W. Scharwaechter and H. Ebener, Acta Metall. Mater. **38** 195 (1990).
[45] T. Richeton, P. Dobron, F. Chmelik, J. Weiss and F. Louchet, Mater. Sci. Engng. A, submitted (cond-mat/0512301).
[46] J.P.K. Sethna, A. Dahmen and C.R. Myers, Nature **410** 242 (2001).
[47] B. Sprusil and F. Hnilica, Czech. J. Phys. B **35** 897 (1985).
[48] T. Kleiser and M. Bocek, Z. Metallkde. **77** 582 (1986).
[49] H. Neuhäuser, in *Dislocations in Solids*, edited by F.R.N. Nabarro (Amsterdam, North-Holland, 1983), p. 319.
[50] H. Neuhäuser, Phys. Scr. **T49**, 412 (1993).
[51] I. Simonsen, A. Hansen and O.M. Nes, Phys. Rev. E **58** 2779 (1998).

[52] E. Nadgorny, J. Schwerdtfeger, F. Madani, E.C. Aifantis and M. Zaiser, to appear in *Proceedings of the International Conference on Statistical Mechanics of Plasticity and Related Instabilities*, PoS (SMPRI2005)012.
[53] J.M. Lopez, M.A. Rodriguez and R. Cuerno, Phys. Rev. E **56** 3993 (1997).
[54] J.M. Lopez and J. Schmittbuhl, Phys. Rev. E **57** 6405 (1998).
[55] O. Wouters, J.P. Vellinga, J. Van Tijum, *et al*., Acta Mater. **53** 4065 (2005).
[56] M.D. Uchic, Mater. Sci. Engng. A **400–401** 268 (2005).
[57] M.D. Uchic, D.M. Dimiduk, J.N. Florando, *et al*., Science **305** 986 (2004).
[58] D.M. Dimiduk, M.D. Uchic and T.A. Parthasarathy, Acta Mater. **53** 4065 (2005).
[59] D.M. Dimiduk, C. Woodward, R. LeSar and M.D. Uchic, Science, submitted.
[60] R.B. Pond, in *The Inhomogeneity of Plastic Deformation* (Metals Park, American Society of Metals, 1973), p. 1.
[61] A. Needleman and J. Gil Sevillano, Scripta Mater. **48** 109 (2003).
[62] E. Nadgorny, *Dislocation Dynamics and Mechanical Properties of Crystals* (Pergamon Press, Oxford, 1988).
[63] U. Essmann and H. Mughrabi, Phil. Mag. A **40** 731 (1979).
[64] M. Wilkens, Acta Metall. **17** 1155 (1969).
[65] F.F. Csikor, B. Kocsis, Bakó, B. and I. Groma, Mater. Sci. Engng. A **400** 214 (2005).
[66] V.V. Bulatov, M. Tang and H.S. Zbib, 2001, Crystal Plasticity from Dislocation Dynamics, MRS Bulletin, **26**.
[67] L. Kubin, *Computer Modeling of Dislocation-Controlled Deformation*, Encyclopedia of Materials: Science and Technology (Amsterdam, Elsevier Science, 2001).
[68] J. Gil Sevillano, E. Bouchaud and L.P. Kubin, Scripta Metall. Mater. **25** 355 (1991).
[69] M.-C.Miguel, A. Vespignani, M. Zaiser and S. Zapperi, Phys. Rev. Lett. **89** 165501 (2002).
[70] M.-C. Miguel, P. Moretti, M. Zaiser and S. Zapperi, Mater. Sci. Engng. A **400** 191 (2005).
[71] E.N. Andrade da C., Proc. R. Soc. London A **84** 1 (1910).
[72] E.N. Andrade da C., Proc. R. Soc. London A **90** 329 (1914).
[73] A. Pertsinidis and X.S. Ling, New J. Phys. **7** 33 (2005).
[74] M. Zaiser, B. Marmo and P. Moretti, in *Proceedings of the International Conference on Statistical Mechanics of Plasticity and Related Instabilities*, PoS (SMPRI2005)053.
[75] O. Perkovic, K. Dahmen and J.P. Sethna, Phys. Rev. Lett. **75** 4528 (1995).
[76] M. Zaiser and P. Moretti, J. Stat. Mech. P08004 (2005).
[77] G. Picard, A. Ajdari, F. Lequeux, *et al*., Euro. Phys. J. E **15** 371 (2004).
[78] M. Zaiser and E.C. Aifantis, Int. J. Plasticity, in press.
[79] I. Groma, F. Csikor and M. Zaiser, Acta mater. **51** 1271 (2003).
[80] J.-C. Baret, D. Vandembroucq and S. Roux, Phys. Rev. Lett. **89** 195506 (2002).
[81] V.V. Bulatov and A.A. Argon, Model. Simul. Mater. Sci. Engng. **2** 167 (1994).
[82] G. Picard, A. Ajdari, F. Lequeux, *et al*., Phys. Rev. E **71** 010501 (2005).
[83] M. Koslowski, A.M. Cuitino and M. Ortiz, J. Mech. Phys. Solids. **50** 2597 (2002).
[84] M. Koslowski, R. LeSar and R. Thomson, Phys. Rev. Lett. **93** 125502 (2004).
[85] Y.U. Wang, Y.M. Jin, A.M. Cuitin and A.G. Khachaturyan, Acta mater. **49** 1847 (2001).
[86] R.A. White and K.A. Dahmen, Phys. Rev. Lett. **91** 085702 (2003).
[87] K. Chen, P. Bak and S.P. Obukhov, Phys. Rev. A **42** 625 (1991).
[88] A. Middleton, Phys. Rev. Lett. **68** 670 (1992).